DIFFUSE OPTICAL IMAGING OF BRAIN FUNCTION UNDER

REPETITIVE TRANSCRANIAL MAGNETIC STIMULATION

AND IN CHILDREN WITH CEREBRAL PALSY

by

SAMEER C. DHAMNE

Presented to the Faculty of the Graduate School of

The University of Texas at Arlington in Partial Fulfillment

of the Requirements

for the Degree of

MASTER OF SCIENCE IN BIOMEDICAL ENGINEERING

THE UNIVERSITY OF TEXAS AT ARLINGTON

December 2009

ACKNOWLEDGEMENTS

ABSTRACT

DIFFUSE OPTICAL IMAGING OF BRAIN FUNCTION UNDER

REPETITIVE TRANSCRANIAL MAGNETIC STIMULATION

AND IN CHILDREN WITH CEREBRAL PALSY

Sameer C. Dhamne, M.S.

The University of Texas at Arlington, 2009

Supervising Professor: Hanli Liu

Diffuse Optical Imaging (DOI) is a non-invasive neuroimaging technique which measures the changes in oxy- and deoxy-hemoglobin concentrations at a high temporal resolution based on the principle of Near-Infrared Spectroscopy.

DOI was combined with repetitive Transcranial Magnetic Stimulation (rTMS) to assess the neuronal changes induced in the cortical regions, which are directly under rTMS and the connected areas, by applying 1Hz rTMS to the left hemisphere of the motor cortex followed by the stimulation to the prefrontal cortex for two visits. The DOI signals were simultaneously acquired from both ipsilateral and contralateral brain regions before, during, and after rTMS. We observed that there was no significant difference in the temporal responses between visit 1 and visit 2. Stimulation of both the cortices resulted in a significant decrease in oxy-hemoglobin concentration in both the ipsilateral and contralateral sides, which showed high temporal consistency. Also functional connectivity between the stimulated site (at the selected seed

region) and the contralateral regions was investigated by performing a correlation analysis of the DOI time series using seed-region correlation mapping. The correlation maps exhibited a remarkable degree of temporal synchronization between the two hemispheres in both motor and prefrontal cortex, confirming that rTMS generated strong inter-hemispheric effects during and after rTMS.

In another clinical study, DOI and Electromyography (EMG) were employed together to assess the cortical activity and reorganization in children affected with Cerebral Palsy (CP), a motor impairment. The results showed that the functional connectivity patterns along with EMG responses for a finger-tapping protocol differentiate the brain activity in healthy and CP children. Finally in a pilot study, the feasibility of a simultaneous functional MRI (fMRI) and DOI approach was tested to validate the DOI results with fMRI yielding high consistency between the two.

TABLE OF CONTENTS

LIST OF ILLUSTRATIONS

LIST OF TABLES

CHAPTER 1

INTRODUCTION

1.1 Near-Infrared Spectroscopy (NIRS)

1.1.1 Principles of NIRS / Diffuse Optical Imaging (DOI)

Absorption and elastic scattering are the two predominant characteristic interactions of the visible light and near-infrared (NIR) light with biological tissues. The absorption spectra of each chromophore molecule is unique, especially oxy-hemoglobin (HbO, Oxy-Hb) and de-oxy hemoglobin (Hb, Deoxy-Hb) which differ markedly. The changes in hemoglobin concentrations can act as an indicator of changes in blood volume and oxygenation in the tissue of interest. Absorption coefficient (the number of absorption events occurring per unit length, μa) contains maximum physiological information. However, the scatter coefficient (the number of scattering events occurring per unit length, $\mu s'$) in tissue is generally considerably larger, hence the signals measured over distances of a few millimeters or larger are dominated by diffuse light.

Different absorption spectra of HbO and Hb are regularly exploited in physiological monitoring techniques such as pulse oximetry and near-infrared spectroscopy (NIRS). NIRS is an optical modality that measures the attenuation of the biological tissues in NIR spectrum by measuring changes in the concentrations of Oxy-Hb and Deoxy-Hb [1]. Diffuse optical imaging (DOI) is a non-invasive imaging technique used for studying brain activations based which is based on the principle of NIRS. DOI methods use a grid of 1 interlaced source-detector pairs with overlapping measurement volumes, such that each detector receives light from multiple distinguishable sources (refer fig 1.1). The photons in the brain generally take up the banana-

1

shaped path between the source and a detector. The ultimate goal of this imaging technique is to process this information further to produce spatially resolved images. These images display the specific changes in Oxy-Hb and Deoxy-Hb as an indicator of blood volume and oxygenation [2]. In order to filter the undesired hemoglobin changes arising from various physiological factors, functional optical brain imaging requires a faster data acquisition rate. By covering larger brain areas; such spatial coverage is not limited to the activation area but extended to the areas that are not involved with the stimulation, thus providing with some contrast between regions of activation and surrounding.
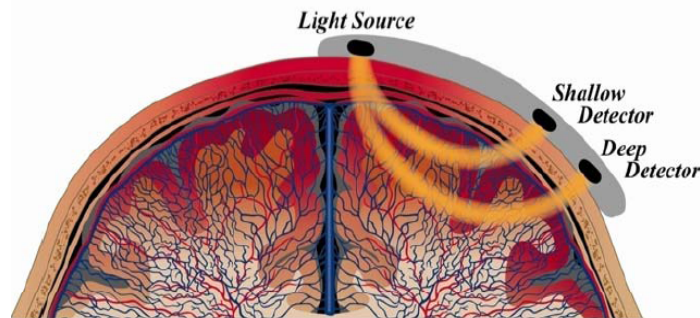
Figure 1.1 Banana-shaped path of photons inside the brain [3]

1.1.2 Optical window

DOI operates at wavelengths in the near-infrared range, around 700 to 900 nanometers. Every molecule or atom has its own characteristic absorption spectra ("spectroscopic fingerprints"). The dominant absorbers in the human body in the visible and near infrared wavelengths are Oxy-Hb, Deoxy-Hb and water. The absorption spectra of these chromophores are shown in Fig. 1.2.

2
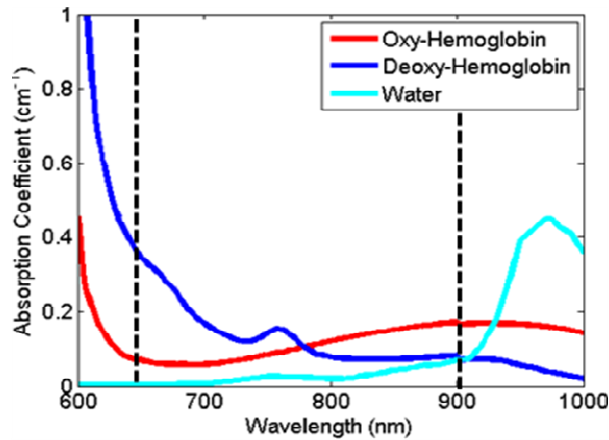
Figure 1.2 Absorption spectra of Oxy- and Deoxy- Hemoglobin [4]

Visible wavelengths of light are strongly absorbed by hemoglobin. This trend decreases significantly for the NIR wavelengths greater than 650 nm. However at longer wavelengths above 950 nm, absorption spectrum of water rises steeply. Thus there is a window between 650 and 950 nm where the absorption of light is small. This spectral range is called a "window of transparency" because it allows light to propagate relatively deeply into the tissue before getting absorbed and, despite the strong scattering of light by tissue the light can diffuse a few centimeters through the tissue and before it is detected. Thus DOI can measure changes in Oxy-Hb, Deoxy-Hb and Total-Hb simultaneously.

1.1.3 Modified Beer-Lambert's Law

Optical absorption changes ΔOD (optical density), is assumed to be small in case of fNIRS/DOI studies. Hence it can be modeled as a linear combination of changes in HbO and Hb as given by the modified Beer-Lambert law (MBLL). The principle of continuous-wave (CW) measurement of hemoglobin concentration in tissue is based on the MBLL. The relationship between the light attenuation and changes in concentrations in tissue from a baseline can be expressed as [6], [7]:

$$OD = \log(Io/I) = \epsilon cL$$

where, OD: attenuation measured in optical densities

      Io: light intensity before the change of concentration

      I: light intensity after the change of concentration

      c: concentration of absorbing species

      ϵ: extinction coefficient of absorbing species

      L: the path length through the tissue.

The path length through the tissue can be decomposed into the source-detector separation (d) and the differential path length (DPF), where L = d * DPF. The differential path length is estimated when using continuous-wave measurements or actually measured for a time-domain or frequency-domain measurements. The source-detector separation can be measured from the probe geometry. The extinction coefficient of the absorbing species, which can be looked up in literature, and the path length the scattered light traveled through the tissue are two pieces that are contained in the proportionality constant.

In order to determine the contribution of HbO and Hb, one must take measurements at one or more wavelengths per chromophore to be resolved. By measuring the changes of optical densities at two wavelengths and using the known extinction coefficients of HbO (ϵHbO) and Hb (ϵHb) at those wavelengths, the concentration changes of HbO and Hb can be thus quantified by solving the two equations with two unknowns as shown below:

$$\Delta[HbO] = (\epsilon Hb^{\lambda 2} * OD^{\lambda 1} - \epsilon Hb^{\lambda 1} * OD^{\lambda 2}) / (L*(\epsilon Hb^{\lambda 2} * \epsilon HbO^{\lambda 1} - \epsilon Hb^{\lambda 1} * \epsilon HbO^{\lambda 2}))$$

$$\Delta[Hb] = (\epsilon HbO^{\lambda 2} * OD^{\lambda 1} - \epsilon HbO^{\lambda 1} * OD^{\lambda 2}) / (L*(\epsilon Hb^{\lambda 1} * \epsilon HbO^{\lambda 2} - \epsilon Hb^{\lambda 2} * \epsilon HbO^{\lambda 1}))$$

$$\Delta[HbT] = \Delta[Hb] + \Delta[HbO]$$

Where, OD $^{\lambda}$: Optical density at wavelength λ

εHbO $^{\lambda}$: Extinction coefficient of oxy-hemoglobin at wavelength λ

εHb $^{\lambda}$: Extinction coefficient of deoxy-hemoglobin at wavelength

1.2 Transcranial Magnetic Stimulation (TMS)

1.2.1 Principles of TMS and repetitive TMS (rTMS)

Transcranial Magnetic Stimulation (TMS) is a non-invasive neuromodulation technique that uses focal alternating magnetic fields over the surface of the brain that pass relatively unimpeded through the skull and into the brain. TMS is basically a bank of capacitors that are rapidly discharged intovan electric coil to produce a magnetic field pulse. When the coil is placed near the head of a human, the magnetic field reaching the cortical areas will generate weak electric currents that further lead to neuronal depolarization, release of neurotransmitters and generation of action potentials. For example, TMS over the left motor cortex causes action potentials that propagate through the corticospinal tract, causing twitches in contralateral skeletal muscles. Repetitive TMS (rTMS) is basically rhythmic TMS applied on a repeated basis at a specific frequency. This involves long continuous trains or short intermittent bursts forming a train of pulses. rTMS can induce changes in neuronal excitability, lasting more than the time of stimulation [7],[8]. Intervening in the course of neurological and psychiatric disorders with rTMS is a growing area of therapeutic development. Gaining a better understanding of how different treatment parameters interact to produce clinical outcome is critical to optimizing the effectiveness of these new treatments. Unlike medications that involve the "parameter space" of only needing to choose whether to use the medication, at which

5

dosage, and for how long, neuromodulation devices like rTMS require the additional choices of where to stimulate, what frequency, what on–off cycle, and for how long [9].
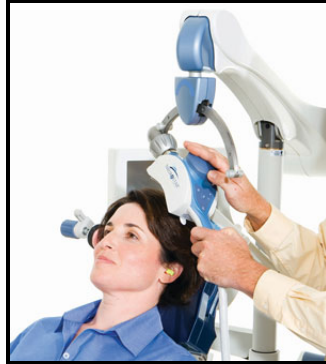
Figure 1.3 TMS system [10]

1.2.2 Coil design and magnetic fields

There are primarily two main types of TMS coils. The circular coils (figure 1.4 (b)), one or more turns of copper set in non-conducting material, with a diameter of 8-10 cm generate a diffuse magnetic field over a relatively large area of cortex. There is little activity under the center of the coil. Instead, activity is strongest under the outer edge of the coil and are hence used for cortical or peripheral stimulation but rarely used in psychiatric treatment. However in case of the figure-8 double coils (figure 1.4 (a)) constructed of two circular coils, about 7 cm in diameter, mounted next to each other are predominantly used in psychiatric treatment. The intensity of the magnetic field drops off sharply with the distance from the center of the field. The volume beneath the junction which is strongly stimulated is of the order of 3 cm long, by 2 cm wide, by 2-3 cm deep, finding its use in application of focal stimulation [11], [12]. A new generation of "coils" are now being manufactured which may be more efficient and provide other patterns of stimulation.

6
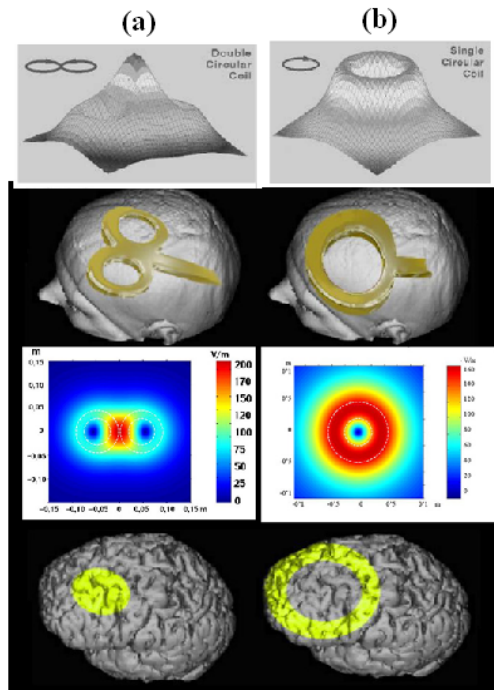
Figure 1.4 TMS coils. (a) Figure-8 coil and magnetic field
(b) circular coil and magnetic field [13]

The strength of the highly localized TMS magnetic field generally is about 1 to 1.5 tesla (approximately equal to the static magnetic field in a magnetic resonance imaging). Irrespective of different coil designs to produce local or diffuse stimulation, the depth of direct stimulation is limited to just below the skull in the superficial cerebral cortex of the brain.

1.2.3 TMS and neuroimaging

The knowledge about the physiologic and pharmacologic actions of TMS is still limited. To understand how rTMS affects cortical activity, research has combined TMS with functional neuroimaging modalities [14], [15] like functional Magnetic Resonance Imaging (fMRI), MRI, Positron Emission Tomography (PET), Near Infrared Spectroscopy (NIRS) and Electroencephalography (EEG). These methods have attempted to address basic science questions of cortical activity and to explore connectivity networks in the brain for the direct

assessment of neural connectivity. In addition to investigating brain function, rTMS is being investigated to also address clinical science questions of therapeutic applications. It has found possible treatment for various brain disorders. As an example, daily prefrontal rTMS has been found to have antidepressant properties when treating patients with depression.

<u>1.3 Brain anatomy and physiology</u>

1.3.1 Neurovascular coupling

Neurovascular coupling is a link between the actual neuronal activity and the associated hemodynamic changes. Since most functional imaging techniques including DOI reflect hemodynamic changes, it is essential to understand the relationship between the two for interpreting functional imaging data and normal brain function.

Neurovascular coupling is a result of the close interaction between neurons, glia, and vascular cells. Ions, metabolic by-products, vasoactive neurotransmitters, and vasoactive factors released in response to neurotransmitters form the basis of the underlying mechanisms of neurovascular coupling [16]–[18]. Astrocytes, a type of glial cell, metabolize glucose by anaerobic glycolysis, leading to lactate production, which is then taken up by neurons and metabolized with oxygen for ATP and CO_2 production. The surrounding capillaries deliver HbO which releases its oxygen and takes away the CO_2, thus converting it to Hb. The K^+ and H^+ ions generated by the extracellular ionic currents caused by action potentials and synaptic transmissions lead to an increased blood flow and volume, causing the smooth muscles in arterioles to hyperpolarize and relax. Moreover the increased blood flow can also be a result of the actions of neurotransmitters, such as acytelcholine released by active neurons, causing the smooth muscles in arterioles to relax. Vasoactive factors released in response to neurotransmitters can also cause vasodilation, such as the activation of glutamate receptors. In

8

this case, intracellular Ca^{2+}, associated with glutamate receptor activation, activates Ca^{2+}-dependent enzymes that produce vasodilators, such as nitric oxide (NO) [16], [17].

Summarizing the whole process (Figure 1.5), it can be said that brain activity is associated with a number of physiological events. Neuronal activity is fueled by glucose metabolism, thus increases in neuronal activity increase glucose and oxygen consumption. On the other hand, a reduction of glucose and oxygen in the capillaries stimulates the brain to increase local arteriolar vasodilation. As a result it leads to an increase of local cerebral blood flow and cerebral blood volume. This mechanism of neurovascular coupling is also driven by the neurotransmitter activity in which the astrocytes are responsible for glutamate recycling. This rate of recycling is proportional to the activity of vasochemical agents. Thus the neurovascular coupling is mediated by neuronal signal mechanism via glial pathways.
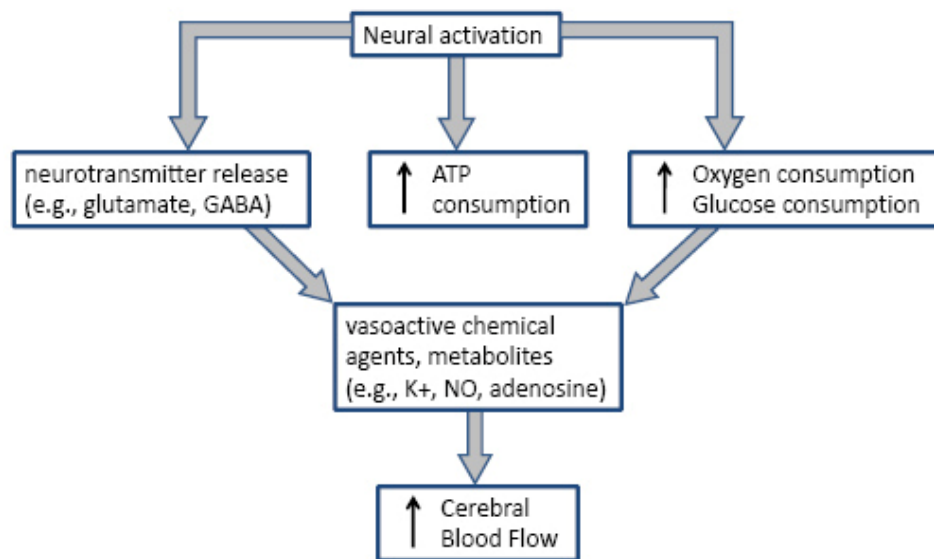
Figure 1.5 Neurovascular coupling

1.3.2 Motor cortex

The human brain is anatomically divided into several cortices. Each cortex is allotted with specific functions. The motor cortex is found in the regions of the cerebral cortex. It is further divided into five areas viz., Primary Motor Cortex (M1), Secondary motor cortex, Premotor cortex, Posterioparietal cortex and Supplementary motor cortex. The primary motor cortex is mainly responsible for controlling the voluntary movements of the body. It functions in coordination with the premotor cortex which plans the execution of movements. The area of interest in our studies is the M1 region which is represented by Brodmann area 4 as highlighted in figure 1.6
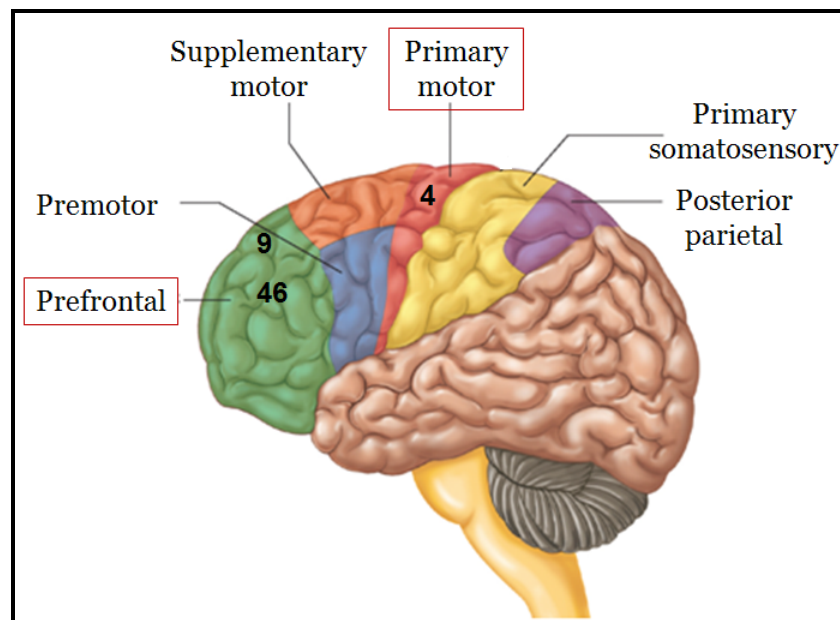
Figure 1.6 Motor and prefrontal cortices

1.3.3 Prefrontal cortex

The prefrontal cortex is located a bit anterior to the supplementary motor area. It is mainly involved in planning cognitive behaviors, personality expression and decision making.

There is much current research devoted to understanding the role of prefrontal cortex in neurological disorders. Many neurological disorders have been related to the dysfunction of the prefrontal cortex. The Dorsolateral prefrontal cortex (DLPFC) is a division of the prefrontal cortex which is represented by brodmann areas 9 and 46. It is amongst the most densely interconnected regions of the association cortes. It projects neurons to both, the cortical as well as subcortical areas. Hence we study the DLPFC to understand the changes in neurological disorders and to come up with techniques to normalize the changes based on what is observed in healthy cortex.

CHAPTER 2

CONCURRENT DOI AND rTMS

2.1 Aim of study

Simultaneously acquiring functional Near Infrared Spectroscopy (fNIRS) during rTMS offers the possibility of directly investigating superficial cortical brain activation and connectivity. By applying rTMS to the left motor and prefrontal cortices and bilaterally recording the fNIRS signals we aim to assess the spatio-temporal changes in the oxy-Hb / deoxy-Hb profiles due to rTMS application. Also we aim to investigate functional connectivity in motor and prefrontal cortices induced by rTMS.

So the goal of the study was to determine if: (1) there were significant differences between Visit 1 and Visit 2; (2) there were significant brain changes associated with motor cortex stimulation; (3) there were significant brain changes associated with prefrontal cortex stimulation; (4) there was concordance between changes in the ipsilateral and contralateral hemispheres; and (5) there were significant differences between the motor and prefrontal cortices.

2.2 Materials and methods

2.2.1. Subjects

The protocol of this study was approved by the Institutional Review Board of the University of Texas Southwestern Medical Center at Dallas. We recruited healthy adult participants (age 18-50 years) who were selected on the basis of not having any history of a

medical disorder and were not on any medication. Prior to study related procedures, subjects provided written informed consent and subsequently underwent a preliminary medical screening by a physician which included Structured Clinical Interview for DSM-IV Axis I Disorders (SCID-I) [19], a Transcranial Magnetic Stimulation Adult Safety Screen (TASS) form [20], medical history review, and a physical exam.

2.2.2. Instruments

2.2.2.1 CW-5 Imager

For DOI, a continuous-wave, MRI compatible Diffuse Optical Imaging system (CW-5, TechEn Inc., MA) was employed with a temporal resolution of 0.1 sec. It is designed to perform multi-wavelength, continuous wave, near infrared, diffuse optical tomographic measurements at very high sampling rates (Fig. 2.1). CW5 system uses frequency-division multiplexed laser sources.

Split evenly between 24 sources, the lasers are at two source wavelengths, 690 nm and 830 nm. The odd numbered lasers function at 690 nm and the even numbered ones at 830 nm. The measured power at the output of laser sources is adjusted as per use. In this project, the 690 nm sources emit near 9 mW and the 830 nm sources near 5 mW power. Having an interval of 200 Hz between adjacent frequencies, the lasers are square-wave modulated at a frequency band ranging from 6.4 kHz to 11 kHz. "Continuous parallel operation of all the sources and detectors allows for rapid data collection." [21].

The CW5 instrument has 24 transmitter channels (lasers sources) and 24 receiver channels (detectors). The unit houses 21 cards: 6 transmitter cards with the four lasers each, 12 receiver cards with two detectors each, one control card with 3 connectors to National

Instrument data acquisition cards, and one clock buffer card. The locations of the twenty-one cards as visible on the front panel of the instrument can be seen in figure 2.1
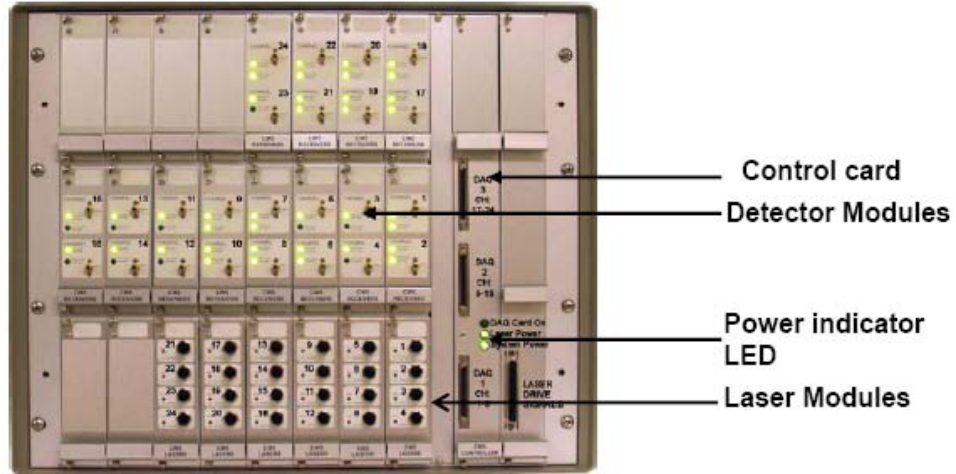
Figure 2.1 Front panel of CW5 imager

The laser source transmitter card and receiver card for the system can be seen in figure 2.2. Each laser source card has four sources, 2 of each wavelength. The system has 6 such cards arranged in parallel on the front panel, giving 12 sources of each wavelength.
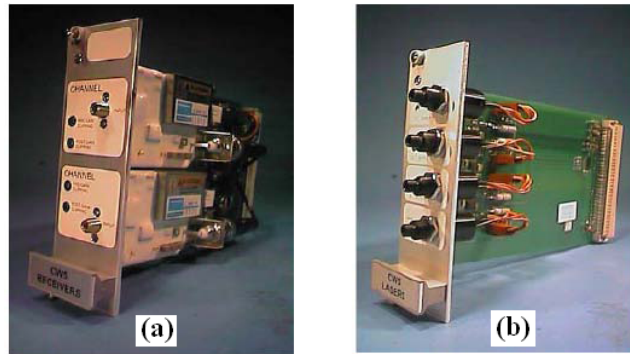
Figure 2.2 (a) Source (b) Detector cards of CW5

There are totally 24 APD detectors present on the system with each receiver card having one APD detector. The 24 receiver channels generate a set of 24 single ended analog signals. The controller (shown in figure-2.5) buffers and converts these 24 single ended signals to 24 differential pairs and drives them out the analog signal connector [21].

14

A thermoplastic DOI probe having 8 sources (diode lasers at 690 nm and 830 nm) and 16 detectors was assembled for optical imaging, forming a total area of 20×6 cm^2 (Fig. 2.3). The sources and detectors were arranged in three rows with the 8 sources being in the middle one and the 16 detectors occupying the first and the last row. By keeping the nearest source-detector distance at 3 cm, we had 28 near neighbor source-detector pairs (channels), 14 of which covered each hemisphere.
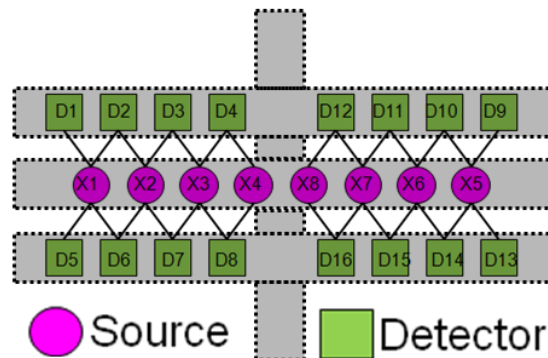
Figure 2.3 DOI probe with sources and detectors

2.2.2.2 TMS machine

A Neuronetics transcranial magnetic stimulation device (Model 2100 CRS, Neuronetics, Inc., Malvern, PA) was used to provide rTMS stimulation. The TMS coil was a new-generation coil basically employing the concept of a figure-8 shaped double coil. The volume of tissue stimulated with the Neuronetic's rTMS coil is typically about 4-cm by 2-cm to a depth of 2-cm from the surface of the scalp [22].

2.2.3. Paradigm

We administered rTMS in a block-designed protocol that comprised 10 seconds of 1-Hz rTMS stimulation and 80 seconds of rest per block. The entire measurement consisted of 15

such blocks at 90 seconds each with an extra pre- and post-stimulation period of 60 seconds (Fig. 2.4). The main advantage of using a block—design is to maximize the signal-to-noise ratio. The total optical imaging acquisition time was 24 minutes and 30 seconds for both the motor and prefrontal corticies. The entire procedure was carried out twice across 2 visits separated apart by 2-3 days.
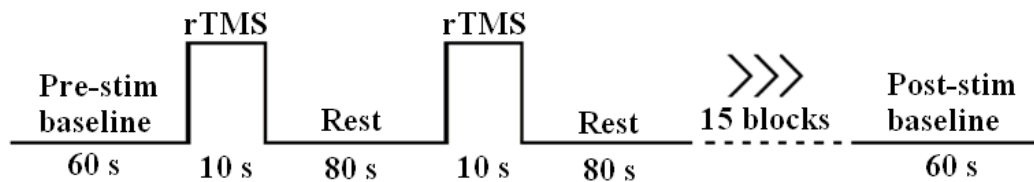
Figure 2.4 Experimental protocol – TMS / DOI

2.2.4 Experimental setup and procedures

An adjustable rTMS system chair was used to position the subjects comfortably for the experiment. First, head-size was measured for each subject and accordingly the DOI probe was positioned bilaterally over the primary motor cortex area. The DOI probe was held tightly over the target area by velcro-and-elastic-bandage strapping such that the optode tips had direct contact with the scalp skin. Furthermore, care was taken to ensure optimal contact between the optodes and scalp by manually moving out the hair under the optodes. For standardized repeatability of DOI probe placement in visit 2, the distance between nasion and the middle row of the DOI probe was measured and recorded.

The location to acquire the motor threshold (MT) was visually determined (Pridmore et al. 1998) as the point of maximal stimulation of the contralateral (right) thumb (abductor pollicis brevis), obtained by applying TMS at the optimal spot over the left motor cortex. Using the T.M.S. Motor Threshold Assessment Tool developed by J. Borckardt and F. Awiszus [23] the motor threshold (MT) was determined three times and averaged. Participants were

16

stimulated at 120% of MT. If the MT was greater than 83% of TMS machine output, a stimulation of 100% TMS machine output was used since that was the highest output of the machine. The TMS coil was set 1.5 cm apart from the scalp to avoid any artifacts that could arise from coil-probe contact. To avoid any contamination in DOI signals, all external light to the room was blocked off and the measurements were performed in dim fluorescent light.
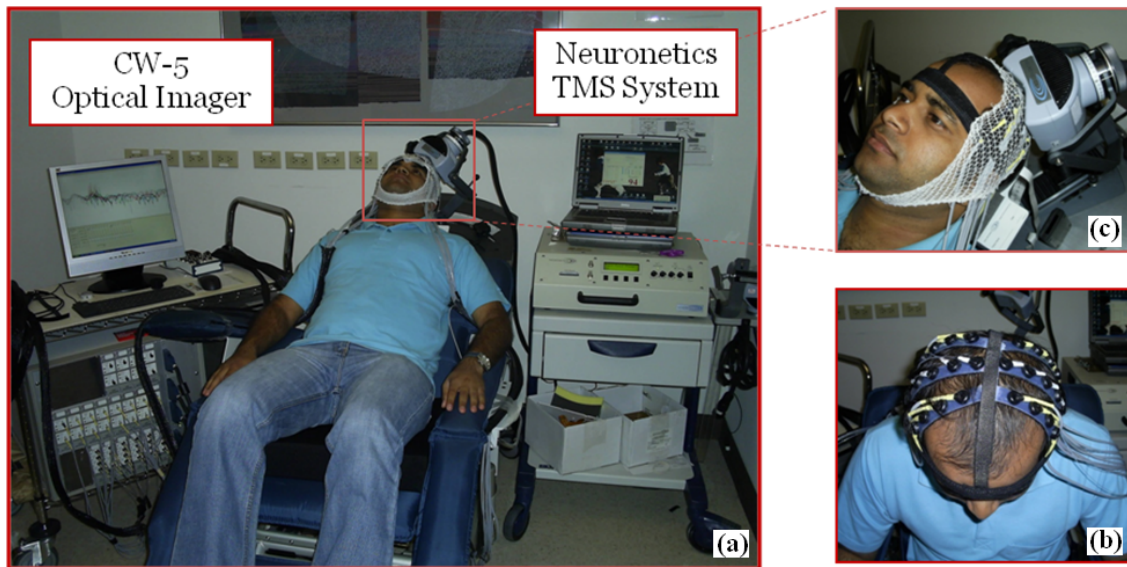
Figure 2.5 Experimental setup with the (a) instruments and subject (b) DOI probe placement on subject's head (c) TMS coil placement on DOI probe

After we set in place the DOI probes and TMS coil, the DOI data was acquired over the motor cortex for the entire protocol. For recording DOI signals over the prefrontal cortex, the DOI probe and TMS coil were repositioned by moving both 5 cm anterior in a para-sagittal line. Using the same stimulation parameters as the motor cortex, simultaneous rTMS and DOI were performed at the prefrontal cortex. After 2-3 days from the first visit, the subjects returned for a second visit of simultaneous rTMS/DOI. The DOI probe was placed at the same position on the motor/prefrontal cortex as in the first visit using the measurements acquired on the first visit. The MT was recalculated to check for any drastic change from visit 1. The MT used in visit 2

was same as that in visit 1 unless there was a change of greater than 10%. Just as during visit 1, the motor and prefrontal cortices were simultaneously stimulated and imaged.

At the end of each recording (motor as well as prefrontal), a TMS spot was determined as the point of direct focal stimulation over the cortex with respect to the DOI probe geometry (e.g. being atop source no.2 or may be in between source 2 and detector 6).

2.3 Data processing

Data processing and image reconstruction was initially performed using commercially available software HomER [24]. The files were then imported to MATLAB for extensive processing.

A check on the quality of acquired optical data was performed by processing the data channel-by-channel (source-detector pairwise). The raw intensities of optical data in each channel were visually checked. Channels that showed large noise without any activation features, possibly due to a subject's thick, dark-colored hair or imperfect probe placement on the scalp, were discarded. We further removed the blocks that exhibited significant motion artifacts. Then, the cleaned data were low pass-filtered (at 0.2 Hz) to remove the instrumental noise/cardiac pulsations. The good blocks across each channel were averaged over all the sessions to obtain Oxy-Hb and Deoxy-Hb temporal profiles. To get the TMS effect from each session, all of the quality checked epochs (90 s) in the session were averaged by channel. Since the probe area of fNIRS on the left hemisphere was larger than the rTMS stimulating area, only the channels directly under the site of stimulation (ranged from 2 to 4 channels based on position of the rTMS with respect to the fNIRS grid) were selected. The site of direct stimulation was slightly variable for each subject. The recorded location of rTMS with reference to the fNIRS determined which channels were used based on the following: four channels were selected if the center of the rTMS coil was positioned directly above a source; two channels

were selected if the center of the rTMS coil was directly over the detectors; and three channels were selected if the center of the rTMS coil was located between the sources and detectors. The reason to utilize a variable number of channels was to maximize the uniformity of the optical signals by only averaging those signals from brain regions directly stimulated. The hemodynamic changes within the selected channels were averaged to get the eventual ipsilateral response under the rTMS coil. Similarly, the mirror channels on the right hemisphere were selected and averaged to get the eventual contralateral response due to rTMS.
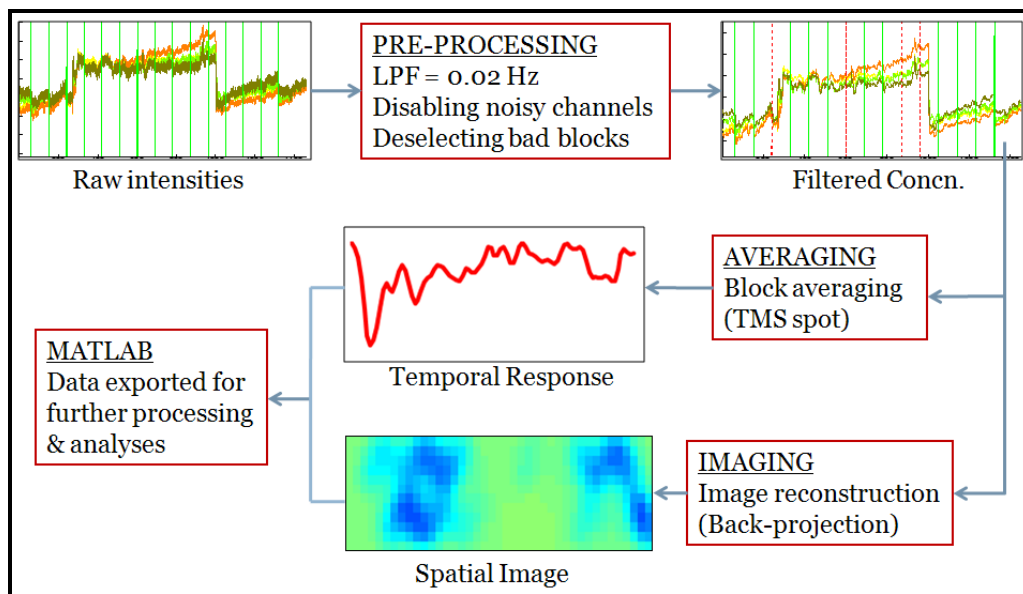
Figure 2.6 Data processing flow-diagram

2.4 Experimental results

2.4.1 Motor cortex

Out of the eleven subjects studied, data of eight subjects were selected on the basis of optimum data quality, for investigating the effects of 1 Hz rTMS stimulation over motor cortex.

The individual responses were averaged across all the subjects (n=8) to obtain a grand-averaged response of Oxy-Hb and Deoxy-Hb changes for all the measurements.

The following figure shows a significant reduction in the Oxy-Hb during stimulation in both the ipsilateral (Fig 2.7 (a)) and contralateral (Fig 2.7 (b)) sides for visit1. Ipsilateral reduction was somewhat lesser than the contralateral reduction. The thumb movement caused by the stimulation confounded the decrease in the signal on the ipsilateral side. Comparable results were observed in case of visit 2 (Fig. 2.7 (c,d)), supporting the reliability of the measure.
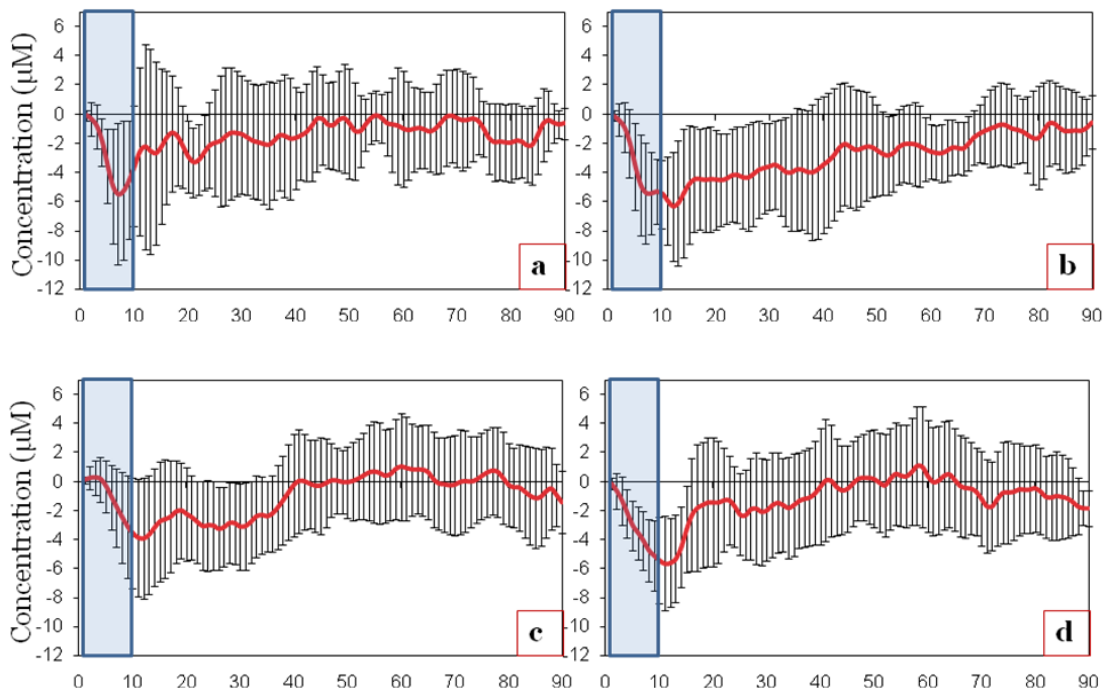
Figure 2.7 Averaged Oxy-Hb temporal responses for motor cortex (a) Visit 1-ipsilateral side (b) Visit 1-contralateral side (c) Visit 2-ipsilateral side (d) Visit 2-contralateral side

Deoxy-Hb exhibited a trend for a minimal increase in the ipsilateral (Fig. 2.8 (a,c)) and contralateral (Fig 2.8 (b,d)) motor cortex, but no significant change in De-Oxy signal was found across the time course. Also the De-Oxy results were similar across both the visits.
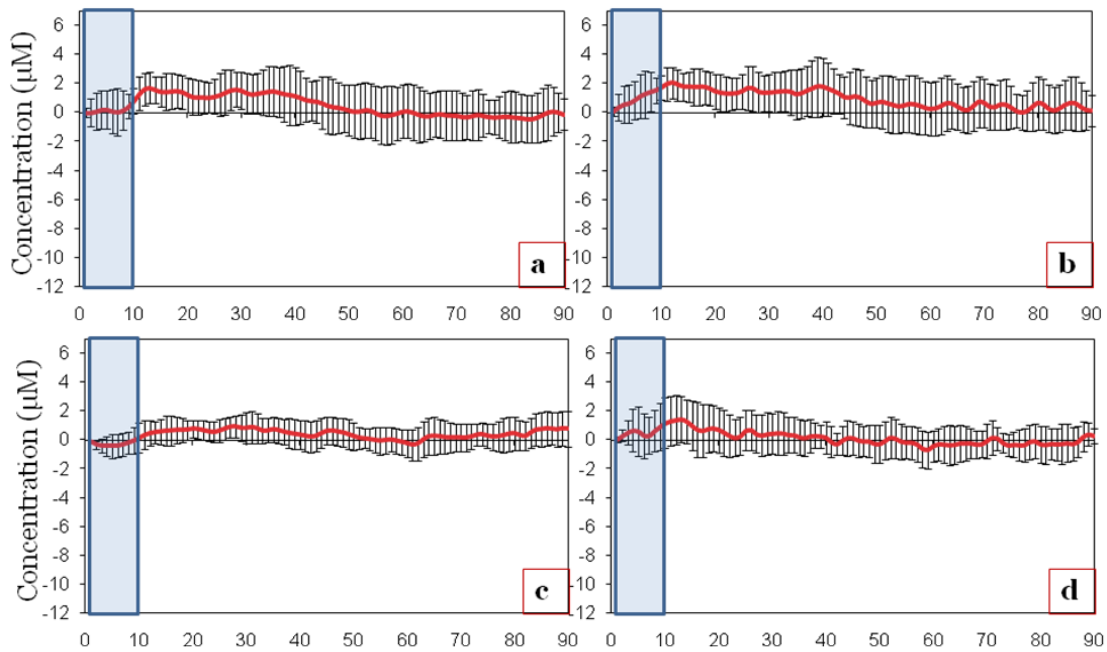
Figure 2.8 Averaged DeOxy-Hb temporal responses for motor cortex (a) Visit 1-ipsilateral side (b) Visit 1-contralateral side (c) Visit 2-ipsilateral side (d) Visit 2-contralateral side

2.4.2 Prefrontal cortex

Based on the data quality, ten out of eleven subjects were averaged to obtain a grand-averaged (n=10) response of Oxy-Hb and Deoxy-Hb changes for all the measurements.

Similar to the motor cortex, a significant reduction in the Oxy-Hb during stimulation in both the ipsilateral (Fig 2.9 (a)) and contralateral (Fig 2.9 (b)) sides was observed for visit1. However the decrease for the contralateral versus the ipsilateral cortices was similar. Comparable results were observed in case of visit 2 (Fig 2.9 (c,d)) supporting the reliability of the measure.

21
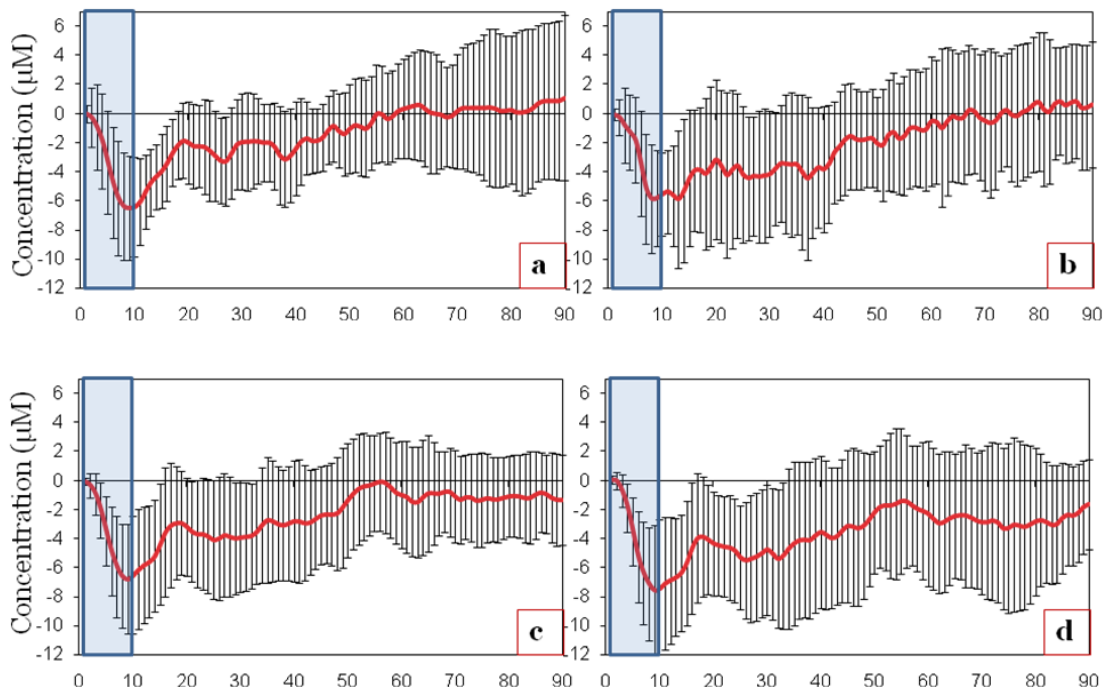
Figure 2.9 Averaged Oxy-Hb temporal responses for prefrontal cortex (a) Visit 1-ipsilateral side (b) Visit 1-contralateral side (c) Visit 2-ipsilateral side (d) Visit 2-contralateral side

Again, Deoxy-Hb exhibited a trend for a minimal increase in the ipsilateral (Fig 2.10 (a,c)) and contralateral (Fig 2.10 (b,d)) prefrontal cortex, but only the ipsilateral cortex was marginally significant. Also the De-Oxy results were similar across both the visits.
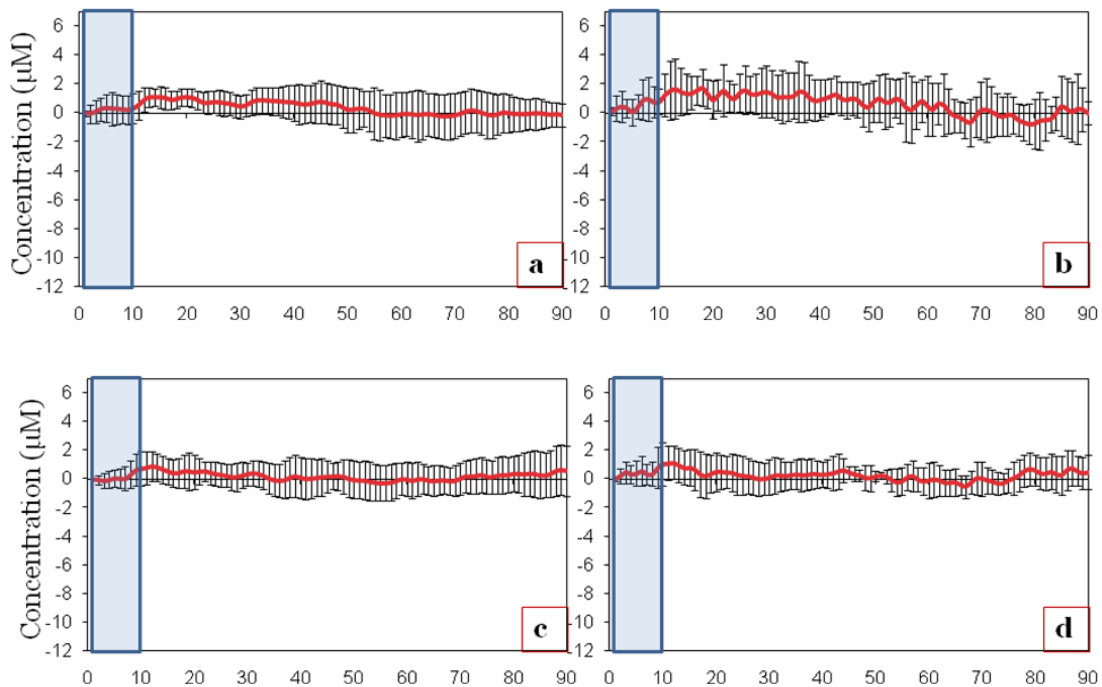
Figure 2.10 Averaged Deoxy-Hb temporal responses for prefrontal cortex (a) Visit 1-ipsilateral side (b) Visit 1-contralateral side (c) Visit 2-ipsilateral side (d) Visit 2-contralateral side

Thus the the brain changes associated with motor cortex stimulation and prefrontal cortex stimulation were very comparable under the conditions studied.

In a clinical setting, prefrontal cortex is the one which would be stimulated to treat for neurological disorders in the patients. So the temporal responses of the ipsilateral prefrontal cortex (Fig. 2.11) would help the doctors to determine the therapeutic changes. These responses to TMS vary in each subject as can be seen in the following figure, causing the TMS therapy to be tailored based on the individual reliability.
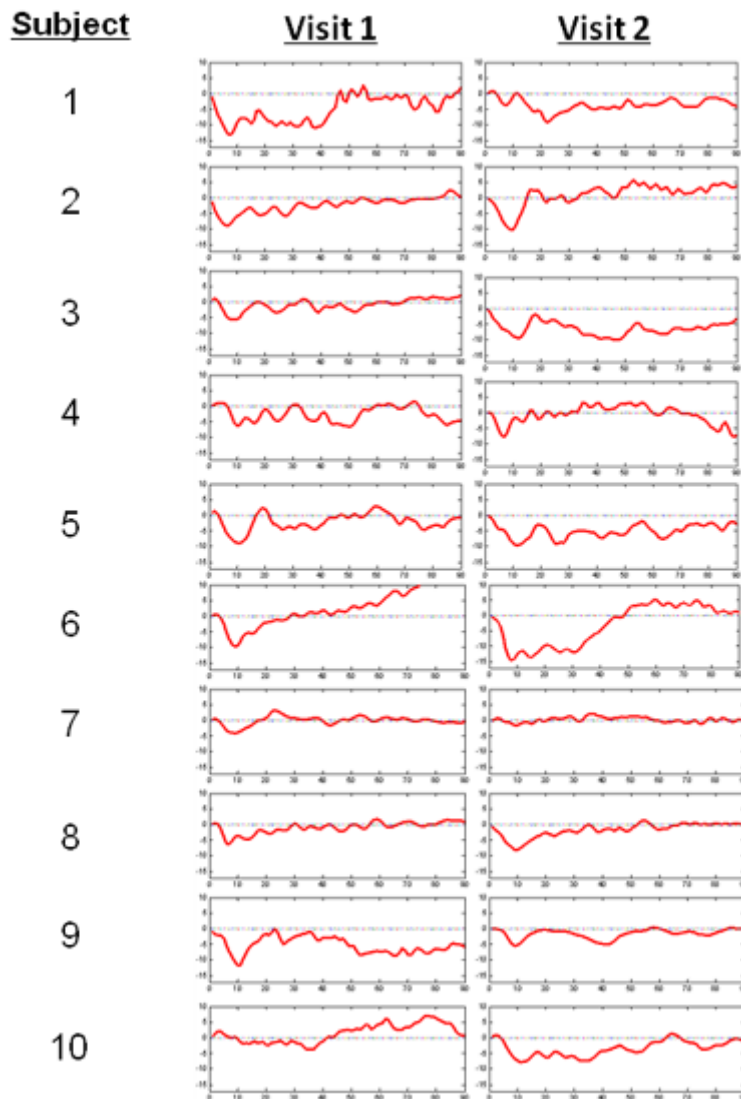
Figure 2.11 Ipsilateral prefrontal cortex temporal responses
for individual subjects

2.5 Multi-parameter analysis

2.5.1 Parameters for temporal analysis

Certain characteristic features of a curve are defined in order to compare and contrast the temporal profiles of brain changes in the motor and prefrontal cortices due to rTMS. These parameters are viz. Correlation coefficient, Peak min, Peak time, Steady State and Area Under the Curve (refer fig. 2.12)

a. Correlation Coefficient (R) - R is the pearson's correlation coefficient calculated between each timepoint of the entire timecourse of two temporal responses. It thus gives an estimate of as to how well the two responses are correlated with each other.

b. Peak min (Pm) – Pm is the local minima of the Oxy-Hb amplitude during the first 35 seconds of the temporal response. It thus gives a single value of the Oxy-Hb change for each response.

c. Peak time (Pt) – Pt is the peak time of the response or the time it takes to reach the Pm value. It thus gives a single time-to-peak value in seconds for a point comparison between the two responses.

d. Steady State (SS) – SS is the average of the Oxy-Hb response over the last 15 seconds of the timecourse. Since the response doesn't reach baseline (zero) in all the measurements, the last 75-90 seconds are considered as the steady recovery of the response. It also gives single Oxy-Hb change amplitude for each measurement.

e. Area Under the Curve (AUC) – AUC is the area formed between the SS value and the temporal response. It thus gives a value which estimates the extent of deactivation in a particular measurement.

All the parameters have been labeled in the following figure.
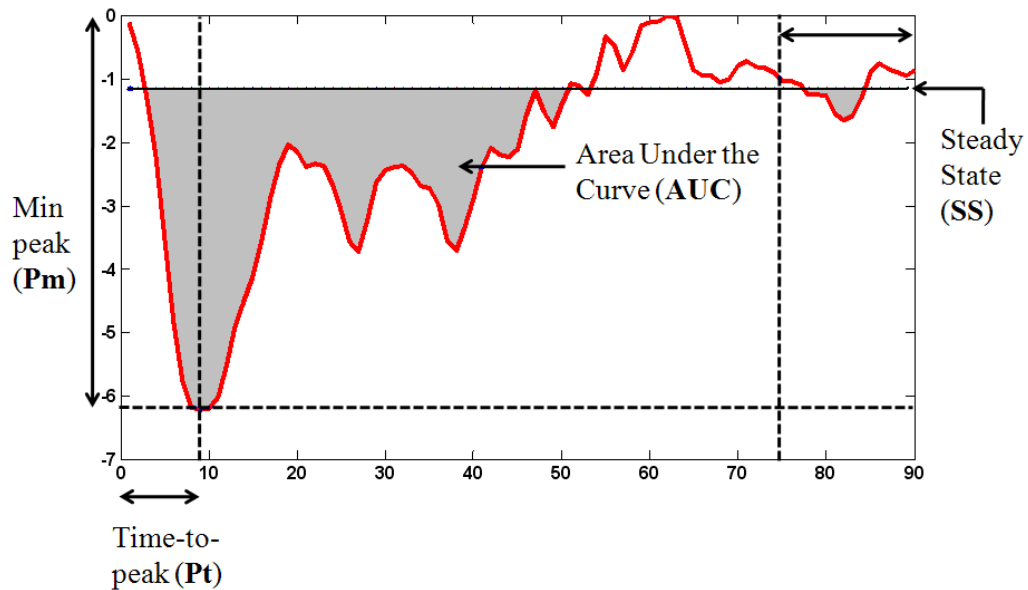
Figure 2.12 Parameters for temporal analysis

2.5.2 Effect of number of epochs

The protocol of study employed 15 epochs of TMS stimulation and rest. As seen in the above sections, rTMS caused a significant decrease of Oxy-Hb level. This result was observed in the data that was block-averaged over 15 epochs. However it would be interesting to determine if a similar effect could be observed, had the protocol consisted only 7 epochs. Also this would enable to answer the question about how long the therapy should be administered to bring out a significant brain change in the individual under the testing conditions. Hence the data was re-processed and re-analyzed to study the effect of number of epochs. This was achieved by comparing 3 datasets for all the subject measurements, viz. a) entire 15 epochs b) first 7 epochs c) last eight epochs. The temporal profiles of all the datasets were plotted and they were compared using the multi-parameter analysis as described in the previous sub-section.

26

2.5.2.1 Fifteen epochs

The following graph is a plot of mean Pm (with standard deviation) of all the measurements. The Pm values have been converted to positive for the ease of comparison. As observed from the graph, Pm has been fairly consistent between the two visits for both the stimulations. The Pm in motor cortex is relatively lower than the prefrontal cortex indicating that the prefrontal cortex (especially the contralateral side) has a bigger dip in the brain activity due to rTMS.
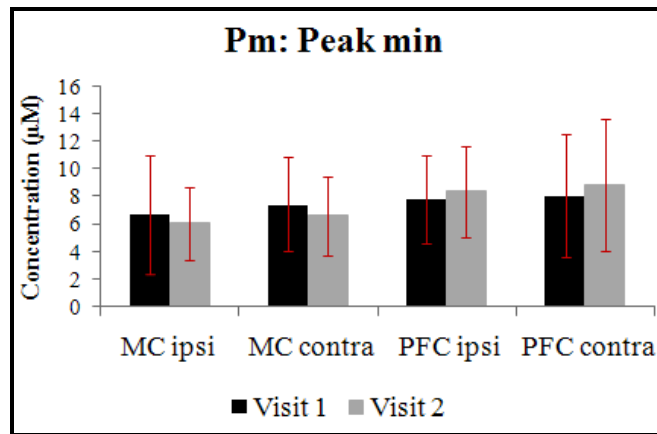
Figure 2.13 Peak min-fifteen epochs

Also the Pt corresponding to Pm has been plotted in figure 2.14. The errorbars indicate standard deviation. Ipsilateral side of the motor cortex has the maximum Pt indicating the slowness of the response to reach its minimum whereas ipsilateral side of prefrontal cortex has the minimum Pt making it the fastest response of all.
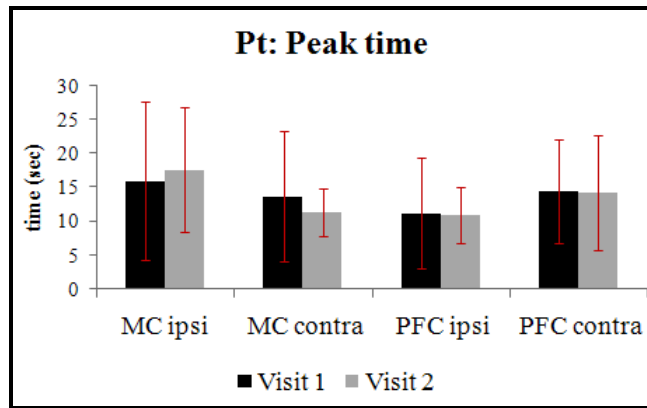
Figure 2.14 Peak time -fifteen epochs

AUC is an indirect measure of the extent of deactivation in a measurement. The graph below indicates the mean AUC for all the measurements. Again due to the thumb movement on the ipsilateral motor cortex, it forms relatively lower area of deactivation between the temporal curve and the SS value. All the remaining measurements show a similar AUC calculation.
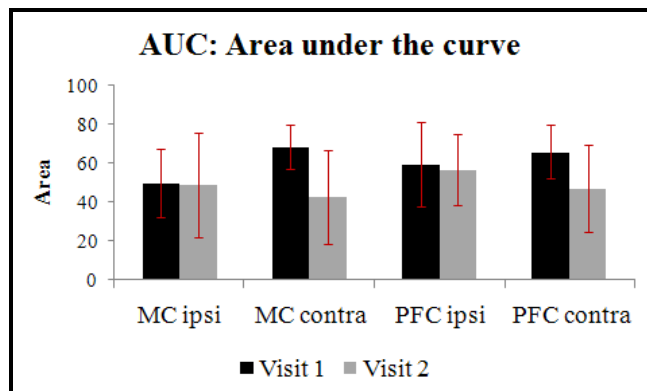
Figure 2.15 Area under the curve-fifteen epochs

In order to statistically compare all the parameters, for each series of measurements, a repeated measures analysis of variance using a general linear models technique was performed on the data. The following table lists the p-values of all parameters.

Table 2.1 Repeated measures GLM – fifteen epochs

Effect	Pm	Pt	SS	AUC
Side	0.5212	0.8186	0.5394	0.5713
Visit	0.9471	0.8945	0.2316	0.0122
Cortex	0.1685	0.3169	0.9973	0.8287

None of the parameters were significantly different in case of side, visit or cortex comparison mainly due to a very large standard deviation in most of the values. AUC shows a significant p value (0.0122) between visits. However that is due the presence of strong interaction in the lower set of comparisons between visit 1 and visit 2 MC contra (p=0.0279). Hence the p-value of AUC at the visit's level can't be considered to be a significant one.

In conclusion, there was no significant difference in the characteristic features of motor cortex and prefrontal cortex responses and are hence very comparable.

2.5.2.2 First seven and last eight epochs

The Peak min comparison between 15, 7 and 8 epochs has been plotted in the figure below. The graphs show some variation in the Pm values for all the three sets of epochs. But on the whole, there doesn't seem to be any difference in the Pm comparisons since it gets averaged out.
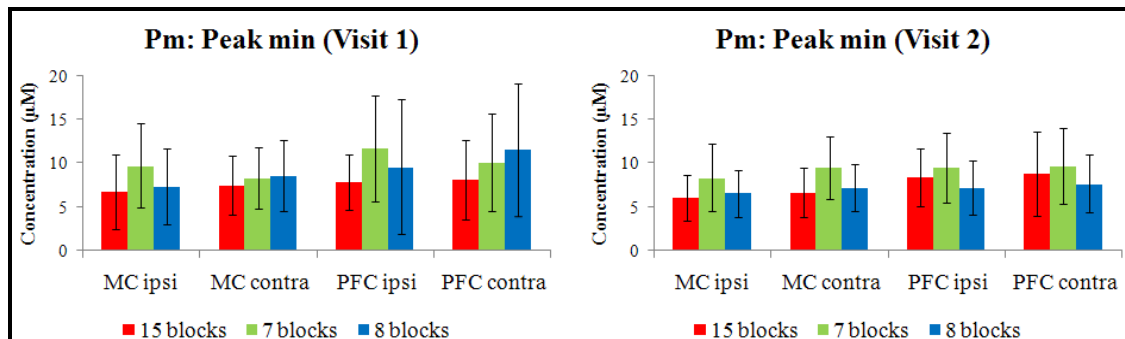
Figure 2.16 Peak min comparisons between different epochs

The following graph does show that time-to-peak is really variable across all the measurements and in all the epochs of comparison. However, no specific conclusion can be inferred due to the large inter-subject variability.
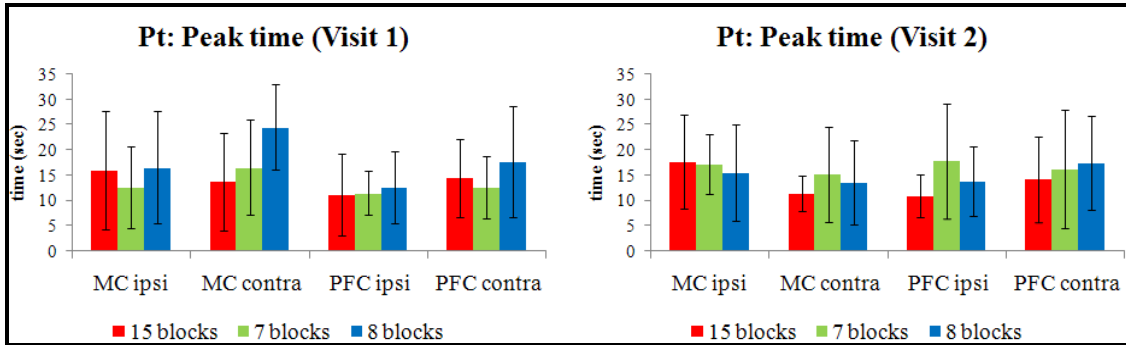
Figure 2.17 Peak time comparisons between different epochs

The next figure plots the AUC values for all the measurements in case of 15, 7 and 8 epochs. The AUC values of 7 and 8 epochs are very comparable to those of 15 showing that the effect of deactivation was achieved in the first seven blocks itself.
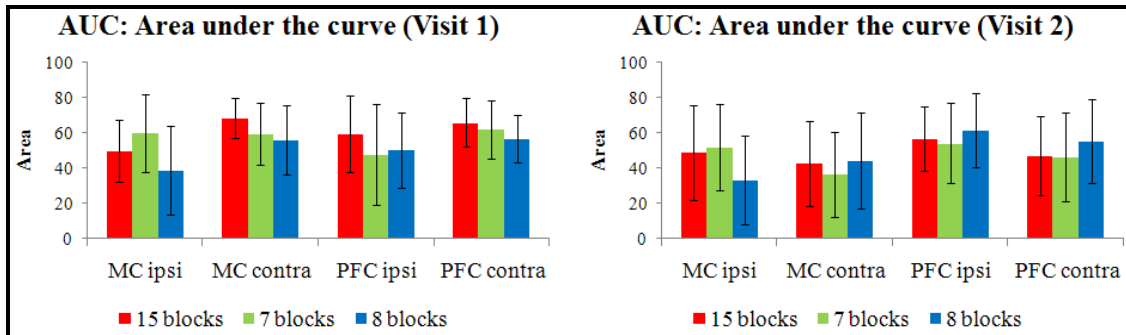
Figure 2.18 AUC comparisons between different epochs

A repeated measures analysis of variance using a general linear models technique was performed on the data to compare between the selections of epochs. The following table lists the p-values of all parameters. None of the parameters was significantly different in case of

side, visit or cortex and blocks (epochs) comparison mainly due to a very large standard deviation in most of the values.

Table 2.2 Repeated measures GLM – seven and eight epochs

Effect	Pm	Pt	SS	AUC
Side	0.6794	0.2434	0.8749	0.5241
Visit	0.0835	0.7749	0.9586	0.1589
Cortex	0.0819	0.2893	0.8315	0.1115
Blocks	0.0795	0.4022	0.7615	0.5241

Thus there was no significant difference between the temporal responses obtained by either averaging fifteen epochs or first seven or last eight. In conclusion, stimulation over 7 epochs does bring out a comparable reduction in the Oxy-Hb levels for all the measurements allowing us to incorporate this information for further studies. Thus, the TMS-induced brain changes can be brought out in a lesser time with only seven epochs.

2.5.3 Effect of Region of Interest (ROI)

The previous analyses were based on the region of interest which was the TMS spot situated just below the site of focal stimulation. In an interest to understand the TMS effects on the brain in areas adjoining the stimulated site, we selected another ROI defined as "non-stim". If the TMS coil was placed between sources X2-X3 and detectors D3-D7, the four non-stim channels (marked in cyan) were selected between source X1 and detectors D1-D2-D5-D6 (refer Fig. 2.19). So these channels in the non-stim region were averaged to perform the further analyses. Also after studying the effects of TMS in the non-stim region, the responses of stim and non-stim regions were compared using the multiparameter approach.
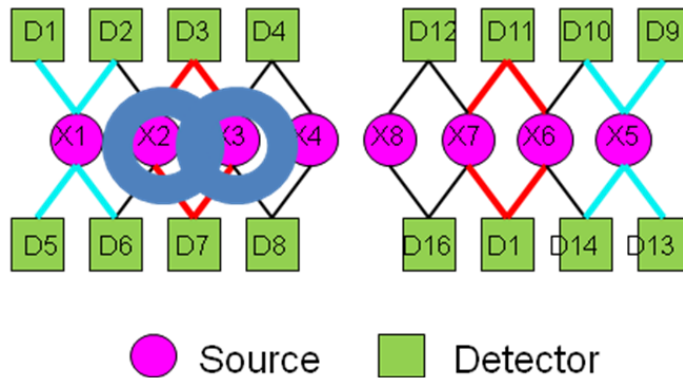
Figure 2.19 Selection of non-stim ROI

The Peak min comparison between Stim and Non-stim ROIs has been plotted in the figure below. The graphs show that there isn't much of a variation between the peaks of oxy-Hb concentration changes in both the ROIs.
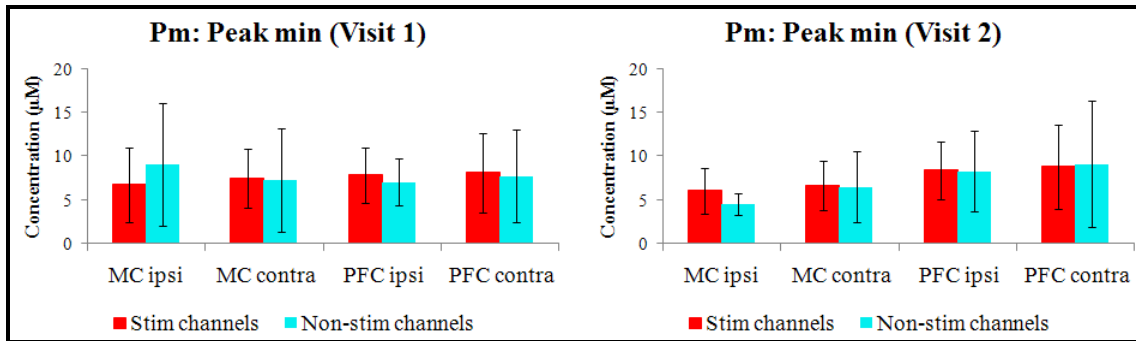
Figure 2.20 Peak min comparisons between different ROIs

The following graph does show that time-to-peak is distinguishable between the two ROIs across all the measurements in two visits. The non-stim channels seem to have a higher peak-time as compared to stim channels implying that the oxy-Hb changes are faster in the stim area as compared to the non-stim area.

32
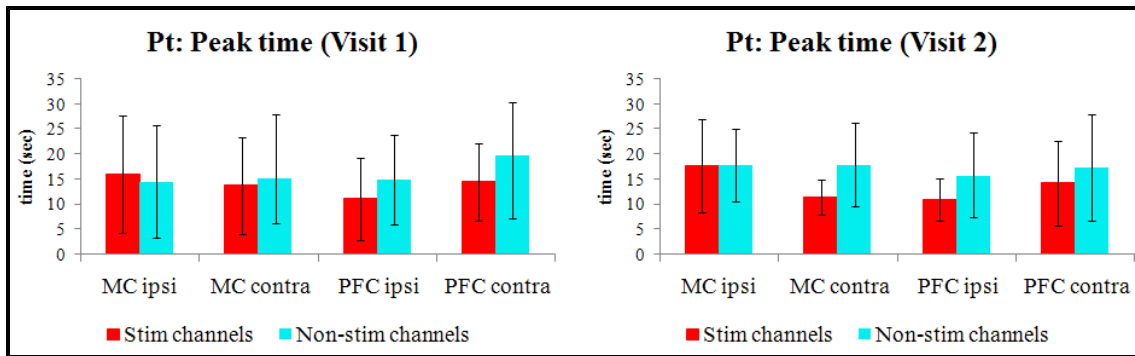
Figure 2.21 Peak time comparisons between different ROIs

The next figure plots the AUC values for all the measurements in case of stim and non-stim ROIs. The extent of deactivation as measured by the area under the curve appears to be different between the two visits for the ROI comparison.
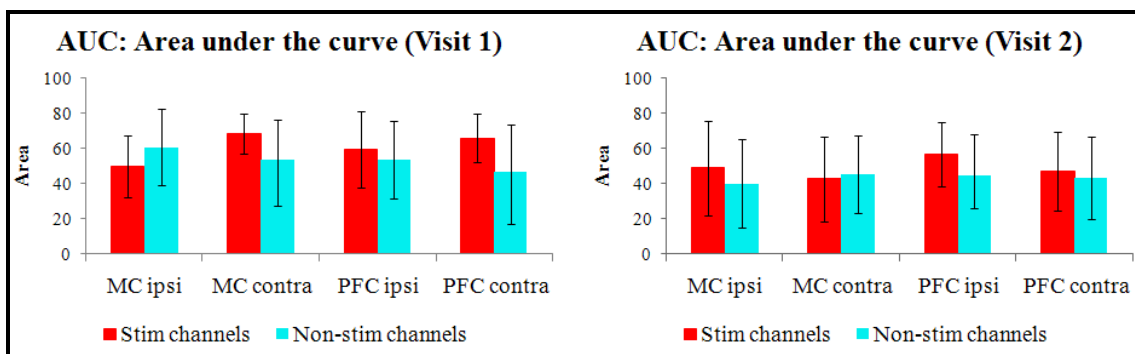
Figure 2.22 AUC comparisons between different ROIs

A repeated measures analysis of variance using a general linear models technique was performed on the data to compare between the various measurements of non-stim ROI. The following table lists the p-values of all parameters and shows that no parameter was significantly different for any measurement.

33

Table 2.3 Repeated measures GLM: Non-stim ROI

Effect	Pm	Pt	SS	AUC
Side	0.4165	0.6856	0.07	0.6647
Visit	0.6161	0.5254	0.7049	0.0717
Cortex	0.9294	0.7625	0.1626	0.4515

A repeated measures analysis of variance using a general linear models technique was performed on the data to compare between the two ROIs. Table 2.4 lists the p-values of all parameters. Only, AUC with p=0.007 was significantly different between the two visits.

Table 2.4 Repeated measures GLM – between different ROI's

Effect	Pm	Pt	SS	AUC
Side	0.481	0.6404	0.0867	0.997
Visit	0.5773	0.7711	0.3296	0.007
Cortex	0.3723	0.4155	0.2749	0.7518
ROI	0.9489	0.0615	0.1838	0.0879

Since TMS stimulates an area of about 4 by 2 cm, the non-stim channels (separated by 2cm) are also stimulated by the TMS. As a result no significant difference I observed in case of stim and non-stim channels in most of the measurements.

2.6 Functional Connectivity

2.6.1 Principles of functional connectivity

Functional connectivity is defined as the temporal correlations between remote neurophysiologic events [25]. It essentially explains how different parts of the brain connect, interact and coordinate with each other in response to a particular task or a cognitive function by mainly focusing on temporal synchrony between those brain regions. Traditionally, functional

neuroimaging studies have focused on task-evoked activations. Functional Connectivity studies offer insight into intrinsic functional networks, complementing the findings of task-based studies [26].

Siebner et al. (2009) demonstrated the combined use of TMS with various neuroimaging tools like Functional Magnetic Resonance Imaging (fMRI), MRI, Positron Emission Tomography (PET), Near Infrared Spectroscopy (NIRS) and Electroencephalography (EEG) to explore connectivity networks in the brain for the direct assessment of neural or functional connectivity. Most of the connectivity studies were limited by task-based protocols that confound the measured connectivity [27], [28]. The task-free method has the advantage of measuring functional connectivity without interference from functional activations. If temporal correlations between a reference site (or the selected seed site) and other regions of the brain exhibit a high degree of functional synchronization, they are considered to be well connected. Such an approach has been reported in the past using various imaging modalities.

There exist several model-based (seed-region correlation mapping, coherence analysis, statistical parameter mapping, granger causality maps, psychophysiological interaction maps) and data-driven (principal component analysis, fuzzy clustering analysis, structural equation modeling, multivariate autoregressive modeling) methods for determination of functional connectivity mainly using fMRI data output [28], [29]. But essentially all these methods represent the notion of covariation or correlation in activity.

In this study we utilized DOI to investigate the inter-hemispheric functional connectivity within the motor and prefrontal cortical areas. To accomplish this, we mapped the spatial distribution of hemodynamic activations in both hemispheres followed by correlation analysis to assess functional connectivity, over the entire period of rTMS and recovery. Such analysis was first introduced into functional neuroimaging by Cao and Worsley [31]. In our

study, we utilized 'Seed-pixel correlation mapping' [29] as a technique to map the correlation coefficients between the complete time series of Oxy-Hb activations in the selected seed region with those from all other pixels.

2.6.2 Data processing and Statistics

The good blocks across each channel were averaged over all the sessions to obtain Oxy-Hb and Deoxy-Hb temporal profiles. A set of two-dimensional (2D) spatial maps of functional activation during and after TMS could be reconstructed at a selected temporal window using the regular backprojection algorithm in HomER software. Specifically, we temporally averaged Oxy-Hb signals over an interval of 10 seconds during and after TMS and presented the spatial maps of cortical deactivation/activation in a temporal evolution format. Such maps or reconstructed images covered the same spatial area as that of the probe with a fixed pixel resolution of 0.5 cm × 0.5 cm. We included only those subjects (n=5 for motor cortex and n=6 for prefrontal cortex) for image reconstruction whose data had optimal quality (at least 22 out of 28 channels having strong signals and 8 good blocks out of 15 in one recording) to be reconstructed for further analysis.

Correlation analysis is one of the most common and simple techniques for studying functional connectivity. Spatial co-location between the DOI pixels and the TMS spot at the site of stimulation were identified in the reconstructed images. A 1 cm^2 area (representing the TMS spot) was selected as the 'seed region' within the DOI spatial maps. This seed region was formed by combining 4 pixels in 2-D which were directly under the site of focal stimulation. The time series of Oxy-Hb from the seed area were averaged and used for correlation analysis. The time series from all other measured pixels were also retrieved from the activation images. After obtaining the entire time series at all other pixels, the correlation coefficient of the time

series was calculated between the seed region and all remaining pixels. Pearson's correlation coefficient, r, was determined as a measure of the correlation. A parametric image of these correlation coefficients was produced [29], [31] which is essentially a single spatial map of the correlation coefficient of each pixel's time series with that of the seed region.

The following figure demonstrates the step-by-step processing of data for functional connectivity analysis.
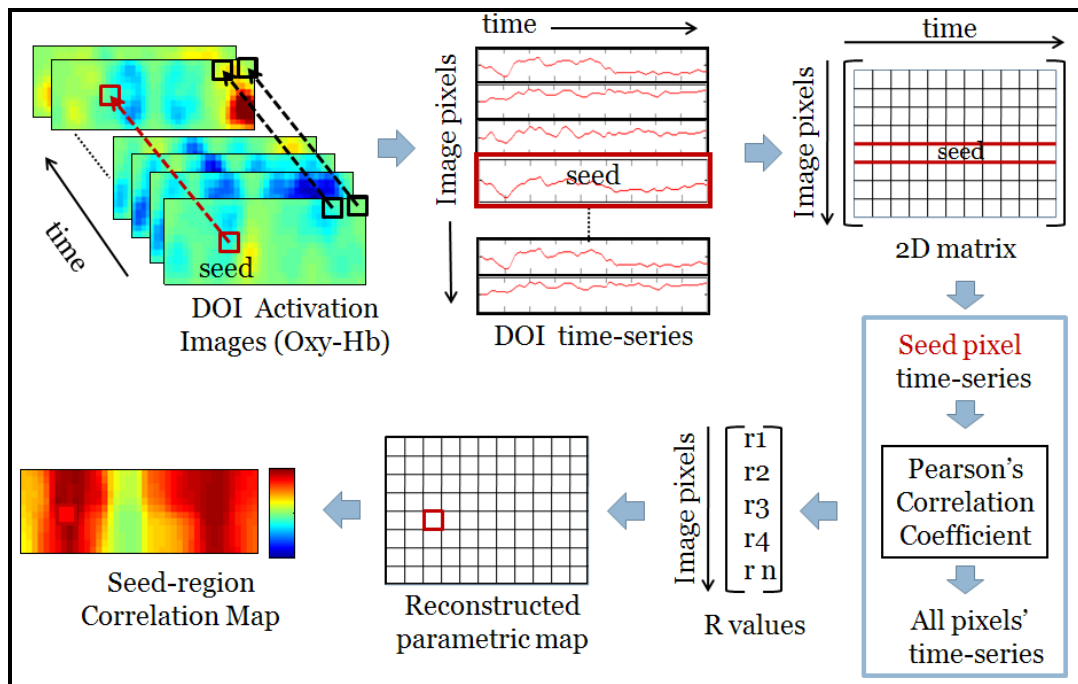
Figure 2.23 Seed-region Correlation mapping

Furthermore, an area of 1 cm^2 (formed by averaging 4 adjacent pixels) was selected on the contralateral cortex, symmetrical to the seed region (marked as mirror-region); a collinear volume of 4 pixels in the centre of the image (defined as central-region) was chosen for statistical comparison.

The *r*-values from the mirror region and central region along with their averaged time courses, across different subjects and measurements, were compared as a means to test the inter-hemispheric correlations in both motor and prefrontal cortices. The 2 sets of *r*-values (for mirror and central regions) in both motor and prefrontal cortex measurements were statistically compared using a paired t-test. The null hypothesis was that the correlation between seed-mirror regions would not be significantly different from that between seed-central regions. Statistical significance was defined as a two-sided p-value of less than 0.05.

As an illustration of the correlation analysis, correlation coefficients were calculated between the averaged time course taken from the seed-region on the ipsilateral side and those taken from all other pixels under the probe for subject 6. While Fig. 2.24(a) represents a functional activation map that was averaged over the stimulation period (1-10 sec), Fig. 2.24(b) shows the correlation image for the same subject with the seed region being selected at the rTMS site. This figure exhibits that the seed region is correlated well with many adjacent pixels ipsilaterally and also with pixels on the contralateral side. To authenticate the correlation image, the time courses of the seed (on the left), central, and mirror (on the right) regions were plotted together in Fig. 2.24(c) to illustrate the temporal synchrony among the three regions. The correlation between the seed and contralateral mirror regions had a coefficient of r = 0.93, indicating very strong synchronization between the two regions. The correlation coefficient between the seed and central region was found to be r =0.18, implying much weaker temporal synchronization between them.
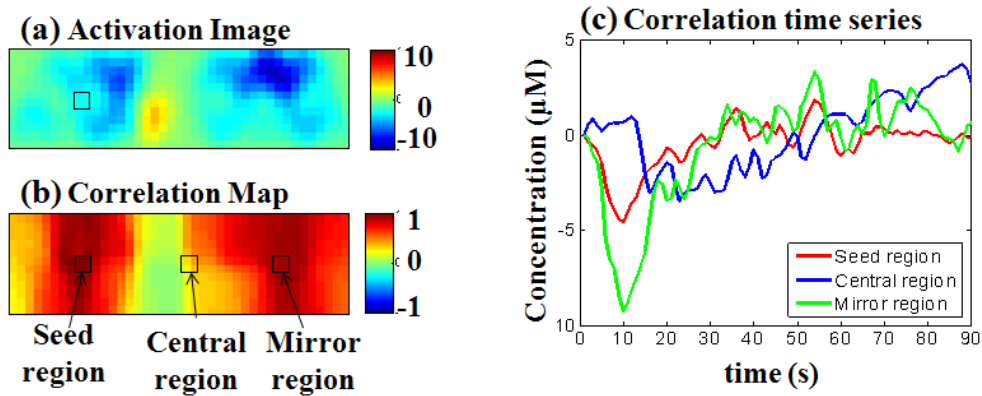
Figure 2.24 Illustration of functional connectivity analysis (a) Activation image (b) Correlation map (c) Correlation time-series

2.6.3 Results

2.6.3.1 Block-averaged functional connectivity

The functional connectivity induced by rTMS was further examined by processing the correlation images from 5 subjects with motor cortex stimulation and from 5 more subjects. So for prefrontal we have 5 (in fig 2.26) and 1 (in fig 2.24)) with prefrontal cortex stimulation.

For the motor cortex stimulation, all the subjects showed bilateral Oxy-Hb deactivation during 1-10 seconds of rTMS application (Fig. 2.25(a)) and strong inter-hemispheric connectivity in the motor cortex (Fig. 2.25(b)). We note that some detailed differences existed in deactivation amplitudes and spatial distributions of connectivity.

39
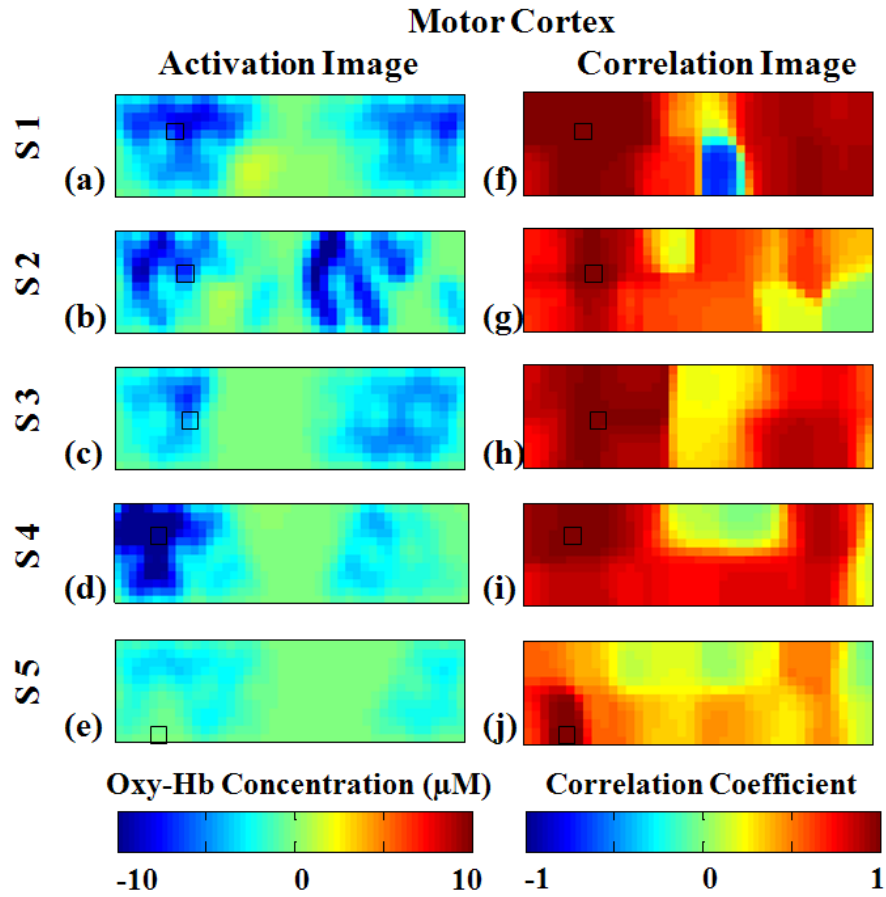
Figure 2.25 Functional connectivity in motor cortex
(a-e) Activation image (f-j) Correlation image

Similarly, the 5 subjects being assessed on the prefrontal cortex revealed a similar trend in reduction of Oxy-Hb in both hemispheres (Fig. 2.26a) and strong inter-hemispheric connectivity in the prefrontal cortex (Fig. 2.26b), while detailed differences are evident in functional deactivation and connectivity. Such differences may be expected and attributed to the individual responses of each subject to rTMS that might result partially from the differences in individual neural anatomy and physiology from each subject.

Figure 2.26 Functional connectivity in prefrontal cortex
(a-e) Activation image (f-j) Correlation image

Statistically, we utilized a paired t-test and concluded that the correlation coefficients, r, between the seed and mirror region of motor cortex (n=5) were significantly greater (t= 3.278, df=8, p=0.0112) than those between the seed and central region. In case of prefrontal cortex (n=6) the r values between the seed-mirror regions were not significantly different from the seed-central region (t=0.3253, df=10, p=0.3253) mainly because of the negative correlation observed in subject#3 between the seed and mirror regions. However by excluding subject#3 (n=5) from statistical calculations, we do observe the seed-mirror correlations to be greater than the seed-central comparison (t=0.6784, df=8, p=0.028). Hence the null hypothesis was rejected, proving statistically that there existed a strong neural connection between the ipsilateral and

41

contralateral hemispheres of motor and prefrontal cortices during and short after rTMS. Figure 2.27 summarizes the means and standard deviations of all the subjects under statistical analysis for both cortices.
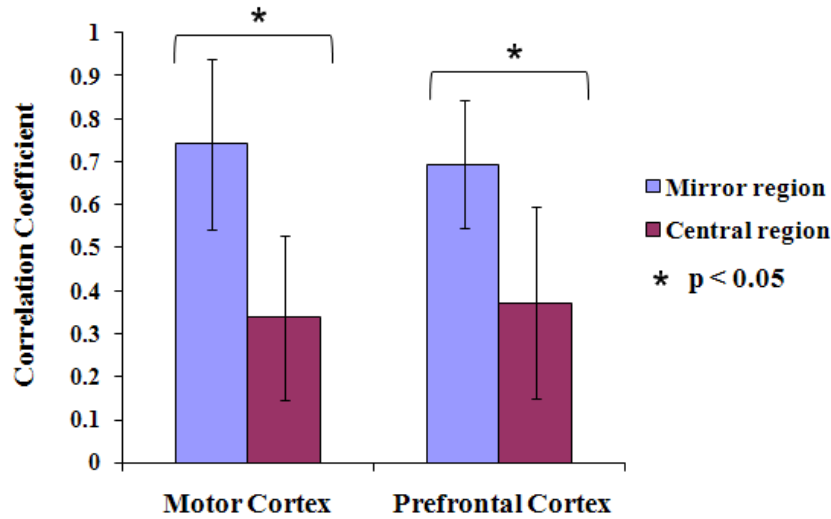
Figure 2.27 Statistical analysis of mean correlation coefficients

2.6.3.2 Resting-state functional connectivity

The last several years have seen growing interest in studying the brain at rest. There is evidence of the existence of an inter-connected neural network in the brain at rest forming the default network. Resting state functional connectivity measures low frequency (< 0.1 Hz) signal fluctuations between regions occurring at rest. These low frequency fNIRS fluctuations are presumed to relate to "spontaneous" neural activity. The major advantages of such studies over task-based studies lie in the fact that task-induced correlations may contaminate the resting correlations, and constant engagement of a task may alter the underlying spontaneous fluctuations.

The purpose of this analysis was to compare the connectivity of the brain at rest and during/after TMS. Also it is important to examine if we were actually measuring the TMS-induced functional connectivity and not the one in resting-state.

The data was processed in a similar fashion as compared to the previous TMS block-averaged connectivity analysis. Additionally it was band-pass filtered (0.02Hz-0.4). It has been shown that the contribution of low-frequency fluctuations was more than 90% of the correlation coefficient and physiological (respiratory and cardiac) noise sources contributed less than 10% to the connectivity maps [32], assuring the selection of filtering frequencies. Again seed-region correlation mapping was used as a technique to compute the correlation map. The selection of seed-region was kept consistent with the previous analysis (TMS spot). The pre-stim baseline of 60 seconds was selected as the DOI time-series for resting state. Though the length of time-series isn't long enough, it can potentially reflect the underlying connectivity.

For the motor cortex stimulation, a remarkable difference was observed between the TMS-induced inter-hemispheric connectivity and the resting state connectivity maps. The TMS block-averaged correlation maps exhibited a stronger pattern of inter-hemispheric connectivity. When the resting state correlation map was subtracted from the TMS correlation map, the difference proved that TMS altered the connectivity network in the motor cortex to induce a high inter-hemispheric spatial distribution of correlation as compared to the resting state. We note that some detailed differences existed in spatial distributions of connectivity across multiple subjects.
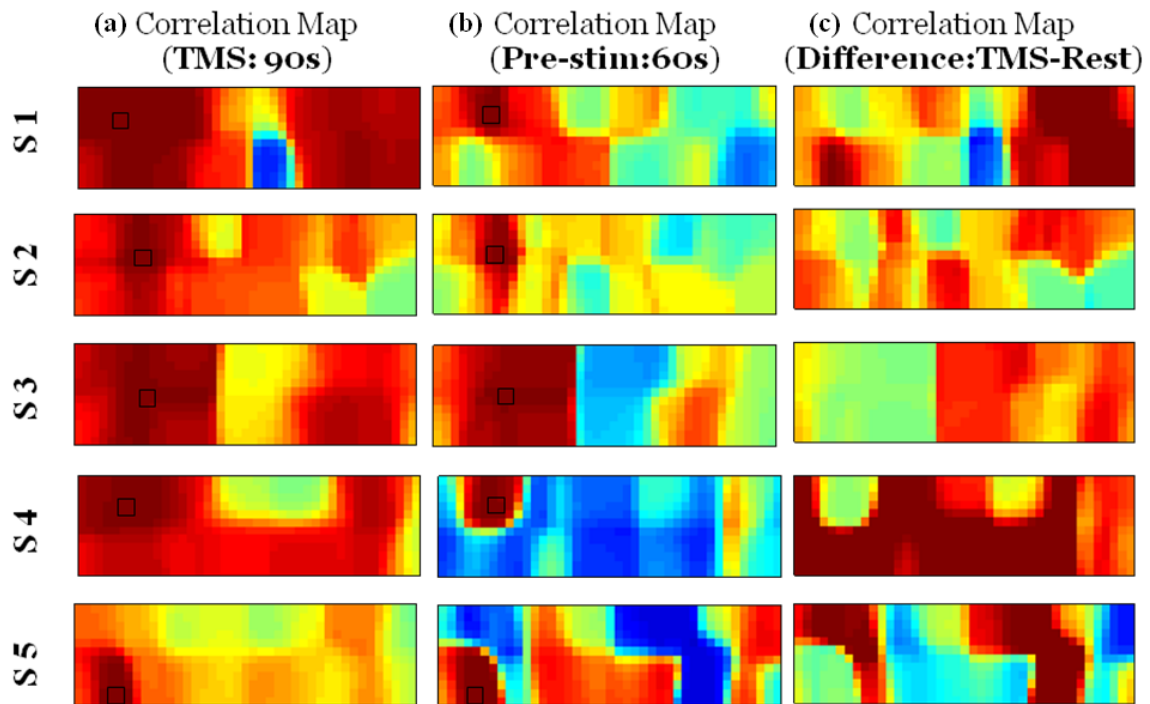
Figure 2.28 Functional connectivity in motor cortex for (a) TMS period
(b) resting-state (c) difference between stimulation and rest

Similarly, the 5 subjects being assessed for the prefrontal cortex revealed a similar difference between the TMS-induced inter-hemispheric connectivity and the resting state connectivity maps. The TMS block-averaged correlation maps exhibited a stronger pattern of inter-hemispheric connectivity, thus proving that TMS alters the connectivity network in the motor cortex to induce a high inter-hemispheric spatial distribution of correlation as compared to the resting state. Detailed differences are evident across subjects which may be expected and attributed to the individual responses of each subject to rTMS resulting partially from the differences in individual neural anatomy and physiology from each subject. Refer figure 2.29.
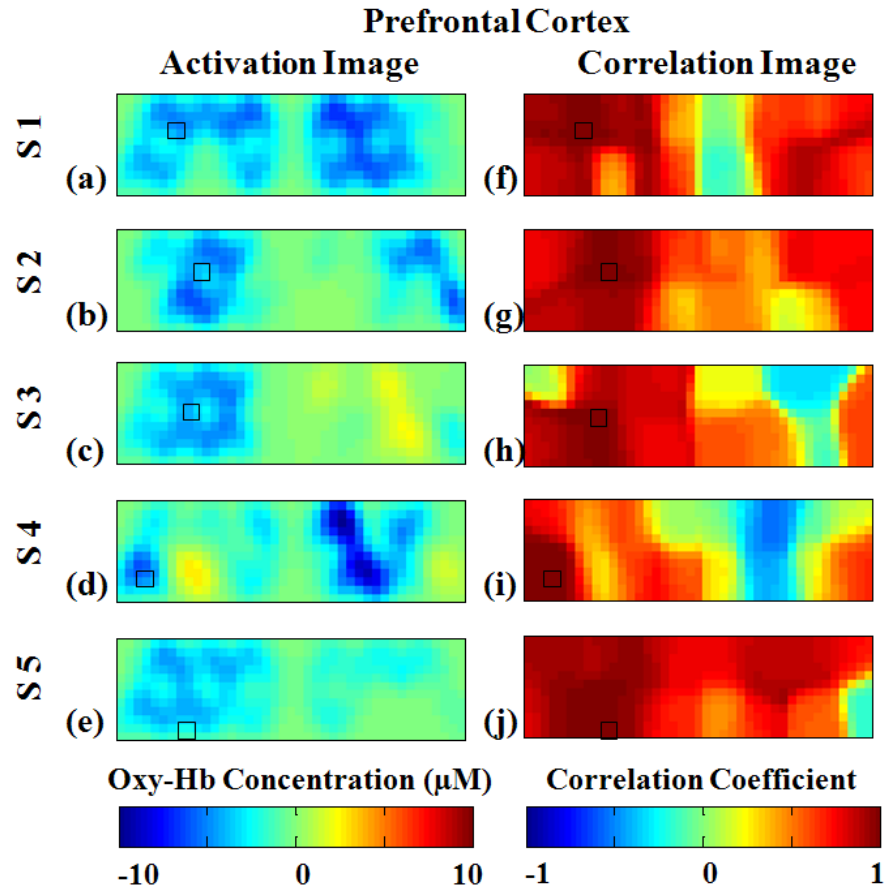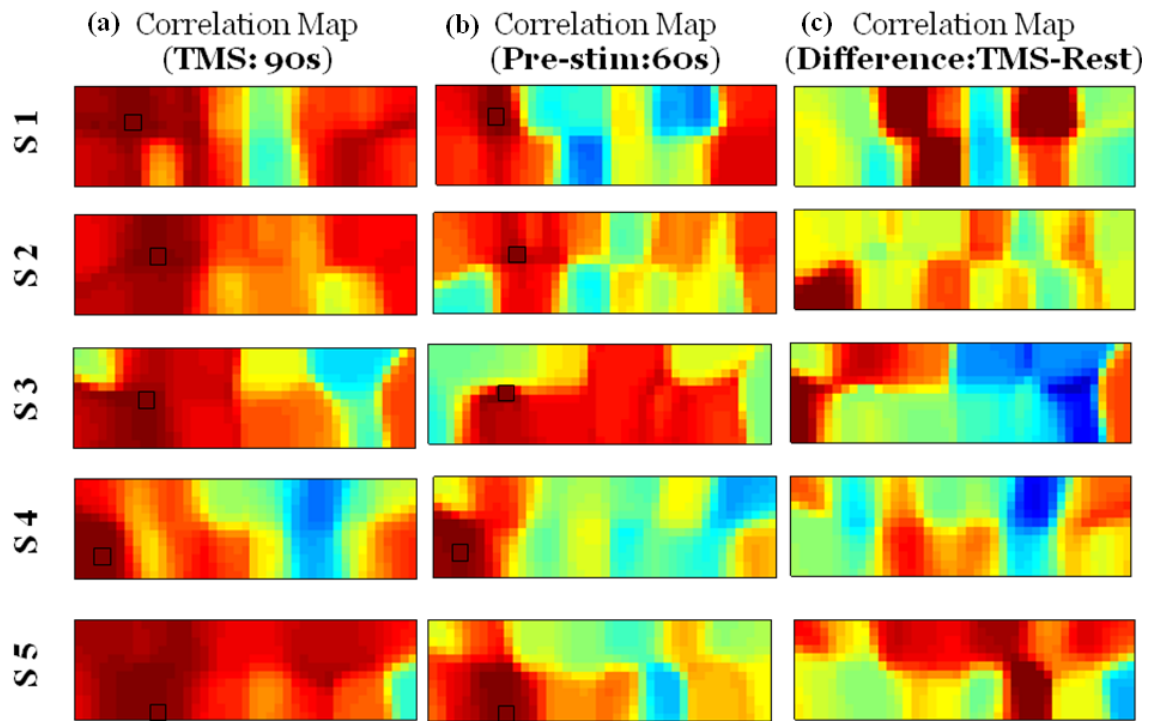
Figure 2.29 Functional connectivity in prefrontal cortex for (a) TMS period
(b) resting-state (c) difference between stimulation and rest

CHAPTER 3

APPLICATION OF DOI / EMG IN CHILDREN WITH CEREBRAL PALSY

3.1 Background of Cerebral Palsy

Cerebral Palsy (CP) is a common disorder causing physical impairment in early childhood. In principle, it refers to a heterogeneous group of disorders arising due to a non-progressive brain disease or a central nervous system (CNS) lesion [33]-[35]. It is in fact caused by a static brain dysfunction or static encephalopathy. At least 2 children per 1000 live births per year suffer from CP. Depending on the severity and type of CP, the motor impairment manifested by the loss of control of movement, coordination and posture ranges from mild to severe [36]. There exist different etiologies explaining the causes of CP during the pre-, peri- and postnatal period. The exact causes are unclear but the main factors that contribute to the defect include very low birth weight and prematurity [37], [38]. Stroke, genetic disease, brain malformation, toxemia, trauma, hypoxic-ischemic encephalopathy and infection placental abruption constitute the other factors [34].

According to the severity of affliction, CP can be divided into 4 types viz. Spastic, Athetoid, Hypotnic/ Ataxic and Mixed CP [34]. Spastic CP is the most frequently diagnosed form of CP which is mainly characterized by rigid and contracted muscles resulting into stiff and jerky movements. Such patients generally find difficulty in moving around and holding on or letting go of objects in hand. It is further classified by the body parts that are affected like Diplegia (both arms or legs are affected), Hemiplegia (limbs on one side of the body are

46

affected) and Quadriplegia (legs, arms, and body are affected). Athetoid CP is the second most common form in which the muscles can either be weak or tight. In addition to the involuntary uncoordinated movements of the face and arms, they are challenged with maintaining upright posture due to low muscle tone. Some patients also suffer from problems related to difficulty in controlling facial muscles causing speech troubles or drooling. Ataxia is the least common cause of CP affecting balance and depth perception due to very weak muscle tone. Patients suffering from ataxic CP often exhibit an unsteady and shaky gait. They experience immense impediment in performing skilled tasks which require control and coordination. The last type of CP is primarily a combination of the above types. The most common mixed type reported is due to spasticity coupled with athetoid movements.

In order to structurally characterize the lesion or abnormality causing any type of CP, novel neuroimaging techniques have been utilized [33], [35]. Magnetic Resonance Imaging (MRI) and Computed Tomography (CT) have shown promise to visualize and diagnose lesions [39]. Since the brain damage due to CP is to some extent a permanent one, none of the current medical techniques can repair the defective brain regions related to motor deficit. Replacing and repairing the injured brain cells or training the brain to develop neuronal pathways present us with some futuristic alternatives to undo the injured brain. With the emergence of a varied range of physical, occupational and constraint-induced therapies or rehabilitative interventions it is however possible to improve the child's ability to use his impaired limbs and increase the efficiency of muscle movement [40].

Thus even if neuroimaging provides an insight into the anatomical abnormalities and rehabilitative methods help in improving the quality of life, they still leave us with an unclear understanding of the cause, variability in the correlation of neuropathology to morphology and inconsistency in descriptions of treatment outcome [39].

47

Owing to the brain injury or lesion, a considerable amount of cortical reorganization has been discovered to take place in the damaged human brain. The healthy hemisphere plays a key role in this neuronal adaptation after the lesions in the central motor system. In most cases of hemiparetic CP, the motor representations of the affected limb are relocated to the hemisphere of the healthy limb [41]. This common finding in neurophysiological investigations is again dependent on various factors like the location, extent of lesion and developmental stage of nervous system. Thus neuroplasticity in young children is essentially a result of adaptation to the abnormal development, injury or disease and needs to be imaged to further correlate the cortical organization with function.

Due to the task performance-cooperation required during its use, it is extremely difficult for CP children to stay still inside the scanner without any movements whatsoever. As a result not many studies have been reported using fMRI. In this study we focus on patients with hemiparetic (hemiplegic) CP which is a subdivision of spastic CP in which one side of the body is affected. The arm and/or leg exhibit a loss of voluntary muscle control on either the left or right side. The study design incorporates the inclusion of hemiparetic CP patients specifically to appraise the performance of the afflicted hand in comparison with the unaffected hand. The brain responses elicited to the stimulation tasks would image different fNIRS activation patterns from both hemispheres which can be correlated with the ones generated from healthy subjects to determine the difference between a diseased and healthy brain. Thus fNIRS can be utilized as a tool to explore the possibility of interhemispheric reorganization in the motor system.

3.2 Materials and methods

3.2.1 Subjects

Pediatric subjects, 6-18 years old, were recruited for the study by constituting two groups: Normals (healthy controls) and CP (children with hemiparetic CP) .

Controls: Healthy volunteers from the local community were approached as regards participation in the study. The ones without any known brain defect or a neuromuscular disease met the inclusion/exclusion criteria and were enrolled for the study.

CP: Patients visiting the Texas Scottish Rite Hospital for Children (TSRHC) who were classified on a scale of 1-3 (1 being the best) as to how they used their hands when handling objects in daily living, according to the Manual Ability Classification System (MACS) [42], [43] were considered potential subjects. After assessing their MRI scans, CP patients with hemiparesis of either upper extremity were eligible for participation. Thus in these patients one hand was affected due to CP and the other hand was healthy. However, any patient with skull defects, deep brain stimulator, ventriculoperitoneal shunt or epilepsy was not recruited.

The study protocol was approved by the Institutional Review Board of University of Texas Southwestern Medical Center at Dallas. A written informed consent was obtained from the guardians/parents of the enrolled children during each visit prior to the experiment.

3.2.2 Experimental setup

The following evaluations were performed during a subject visit:

A neurological examination was performed by a physician to evaluate the mental status of the subject by checking his/her reflexes and asking questions about family, school, activities, seeing, speaking and moving. In order to assess the movement of subject's body, a physical examination testing the muscle tone, strength and coordination while moving arms and legs

49

up/down and back/forth was performed. The physician also screened for the subject's ability to roll, sit, crawl, walk, run and jump. After the neurological/physical examination, an occupational therapist evaluated the upper extremity function on a percent scale for the grasp/release, spontaneous functional analysis and dynamic positional analysis as per the Shriners Hospital for Children Upper Extremity Evaluation (SHUEE) [44]. Again the ability to use hands in handling objects in daily activities was tested using the MACS. A nurse then recorded temperature, blood pressure and heart rate to ensure that the subject was in good health and there were no signs of illness whatsoever; height and weight were also noted down for the records.

After the initial procedures, the subjects were seated in a chair which was adjusted to ensure comfort. The nurse then measured and recorded subject's head size. Based on the head dimensions, the DOI probe was placed bilaterally along the parasagittal line covering the primary motor cortex region. The sources and detectors were attached to the subject's head as shown in figure x using hook-and-loop Velcro straps. In order to achieve consistency in probe-positioning at the subsequent visits, the position of the probe relative to the nasion was measured. Care was taken to avoid contamination of fNIRS recording due to ambient light.

Apart from the DOI brain imaging, surface EMG (B&L Engineering Inc., Santa Ana, CA) electrodes were used to monitor muscle movements during the protocol. Sticky electrodes were placed on the extensor and flexor muscles of both the forearms to check if the subject was tapping correctly with an alternation of extension and flexion of wrist using the ipsilateral hand. Also it assisted in recording any unintended muscle movements during the rest period or from the contralateral hand during the task.

50

3.2.3 Protocol

A blocked-design finger tapping stimulation protocol was utilized for this study. Prior to the actual experiment, the subjects were instructed about the protocol in a short training session wherein they reviewed a video of finger tapping and also rehearsed the same. Data acquisition started with a pre-task baseline of 30 seconds. Right hand finger tapping was performed for 15 seconds followed by a rest period of 25 seconds. Such tapping-rest blocks were repeated 10 times and at the end of 10 blocks, baseline was again recorded for 20 seconds (Refer fig 3.1). On a computer screen in front of the chair, subjects could continually see instructions to stay quiet during rest and a pre-recorded finger-tapping video during the task period which helped them in attaining a predetermined tapping frequency of 1.5 Hz.

At the end of right hand finger tapping a short break was given for the subjects to relax and stretch. We then switched the brace to left hand and the pulse oximeter clip to the right hand to start with left hand tapping task following the same paradigm.
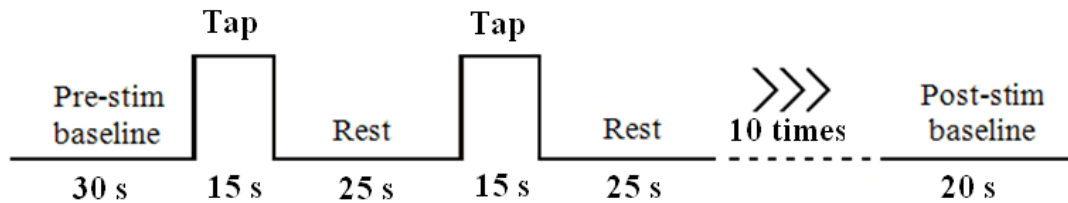
Figure 3.1 Experimental protocol – DOI in CP

3.2.4 Data screening and processing

3.2.4.1 Data screening and performance evaluation

After the 1st visit of a subject, a preliminary processing and analysis of the acquired fNIRS data was performed. The raw intensities of all channels for the entire length of protocol were inspected. There were a few cases wherein the measured optical signals were

51

contaminated and had poor intensities due to light absorption in hair (especially dark colored hair) or due to loose optode-scalp contact. Thus based on the quality of data, the decision to include or exclude the subjects from subsequent visits was made. Only the subjects who recorded good signal intensities were called back to test the reliability of the technique and repeatability of their results.

As a part of data cleaning, all the videotapes of experiments were reviewed together by a team of researchers in several meetings when the recorded sessions of each subject's finger tapping protocol for every visit was watched. The times when the subject made any significant body motion were noted down which included movement of the contralateral limb and/or whole body movement due to yawning or fatigue during the task as well as rest. Also the EMG recordings of both the limbs were simultaneously viewed and again the times when the EMG signals showed an abnormal behavior, were noted down. The optical data in the blocks corresponding to the video-taped body movements and EMG abnormalities were then cross-checked to find for any discontinuities or abrupt changes in the signals and such bad blocks were removed from analysis. Therefore subjects were excluded from analysis due to bad performance or poor cooperation during the task which resulted into too many motion artifacts. Thus by applying an unbiased visuo-technical approach to data screening/cleaning it was ensured that we were analyzing quality-checked optical signals by discarding the data from subjects with poor signal intensity and/or poor performance.

3.2.4.2 Data processing

All the acquired DOI data were preprocessed in a similar fashion as in the rTMS / DOI study (refer fig 2.6). Due to a lot a motion artifacts and poor signal quality from cerebral palsy patients, the temporal analysis wouldn't be a reliable measure of the actual hemodynamic

changes. Hence the Oxy-Hb data was reconstructed to generate spatial images. In this case, the data was block-averaged and the time window of 40 seconds was used for creating the activation images which were representative of the brain activity during the protocol for a subject under consideration. Also based on the seed-region correlation mapping, functional connectivity was mapped in all the subjects using the same algorithm explained in figure 2.23. The pixel of highest activation and the adjoining 3 pixels were selected to form a seed area of 1sq.cm as the seed. Since the subjects were involved in a tapping-task, the task effects would override the underlying functional connectivity. Hence only the initial baseline of 30 seconds was used to create the correlation maps as an indicator of the functional connectivity during the resting state in case of healthy controls as well as the CP patients. Moreover the EMG responses from the CP subjects were plotted on a same scale to reveal the muscle activity during the protocol. All the four EMG responses from the right extensors, right flexors, left extensors and left flexors were plotted in real-time to investigate if there was any bias in the functional connectivity due to some irregular or extra tapping.

3.3 Results

3.3.1 Control subjects

S1 and S2: Left-hand tapping caused an increase in the Oxy-Hb levels in the opposite hemisphere. Thus activation in the contralateral (right) hemisphere was observed as predicted in healthy subjects. Also the correlation maps indicated no inter-hemispheric connectivity between the two sides supporting the observed contralateral brain activation. Similarly, the right-hand tapping led to activation in the left hemisphere of the brain. The correlation maps also showed no inter-hemispheric connections and a pure contralteral brain activity was thus observed.
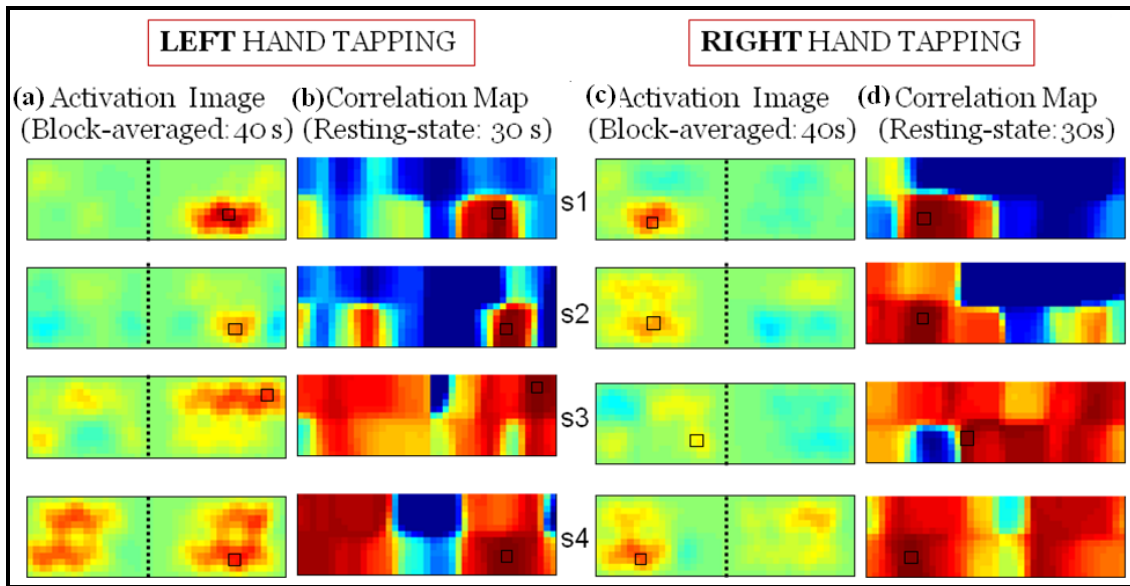
Figure 3.2 Control subjects (a) Left-tapping Activation images (b) Left-tapping correlation maps (c) Right-tapping Activation images (d) Right-tapping correlation maps

S3: Subject no.3 showed a strong bilateral activation during both left as well as right hand finger tapping tasks. Even the correlation maps showed a widespread connection between the two hemispheres supporting the brain activation. This subject, though a healthy control, was on medication for ADHD. Hence an alteration in the brain connectivity networks due to the medicines could be the reason for the observed bilateral activation during an unilateral tapping.

S4: Also subject no.4 showed a strong bilateral activation during both left as well as right hand finger tapping tasks. Even the correlation maps showed a widespread connection between the two hemispheres supporting the brain activation. This subject was a six-year old child. For a six-year old, the brain would still be in a developmental stage. Hence the bilateral response may be elicited due to the activity of the developing brain.

Thus the healthy brain has a contralateral activation and functional connectivity mapping for a unilateral hand tapping with exceptions of ADHD-affected and age-developing brains.

3.3.2 Cerebral Palsy patients

Due to different levels of CP affliction and activation responses elicited by the paretic and non-paretic hand, each CP subject was assessed individually to understand the motor activations and underlying functional connectivity in them.

CP 1 -Right paretic (Fig. 3.3): The right hand of this subject was paretic due to a deformation in the left motor cortex of the brain. When this subject performed finger tapping with his healthy left hand, a contralateral activation (minimally bilateral) was observed. The resting-state correlation map also indicated no interhemispheric connections thus supporting the activations observed. The EMG responses from the left flexors (maroon-bordered) indicated the tapping epochs whereas there was no activity in the right flexors during left hand tapping authenticating that the brain activation was purely due to the left hand tapping. However, with the affected (right) hand tapping, a strong bilateral activation was observed in the motor cortex. The correlation map demonstrated the existence of functional connectivity between the two hemispheres. The EMG responses of the paretic hand (maroon-bordered) showed the inability of the subject to perform equally in comparison of the healthy hand. No EMG activity from the left hand authenticated the existence of inter-hemispheric connectivity while performing right hand tapping. Thus it's a case of cortical reorganization wherein the neuronal pathways between the paretic and healthy hemispheres were rewired.

Figure 3.3 Activation images, correlation maps and EMG responses
of left and right hand tapping for CP 1

CP 2-Right paretic (Fig. 3.4): The right hand of this subject was paretic due to a deformation in the left motor cortex of the brain. When this subject performed finger tapping with his healthy left hand, a bilateral activation was observed. The resting-state correlation map also indicated bilateral connectivity between the two hemispheres. The EMG responses from the left flexors (maroon-bordered) indicated the tapping epochs whereas there was no activity in the right flexors during left hand tapping authenticating that the brain activation was purely due to the left hand tapping. However, with the affected (right) hand tapping, a stronger bilateral activation was observed in the motor cortex. The correlation map also demonstrated the existence of functional connectivity between the two hemispheres. The degree of connectivity was stronger in this case since the damaged hemisphere must have recruited response from the healthy hemisphere to perform the task. No EMG activity from the left hand authenticated the existence of inter-hemispheric connectivity while performing right hand tapping.

56
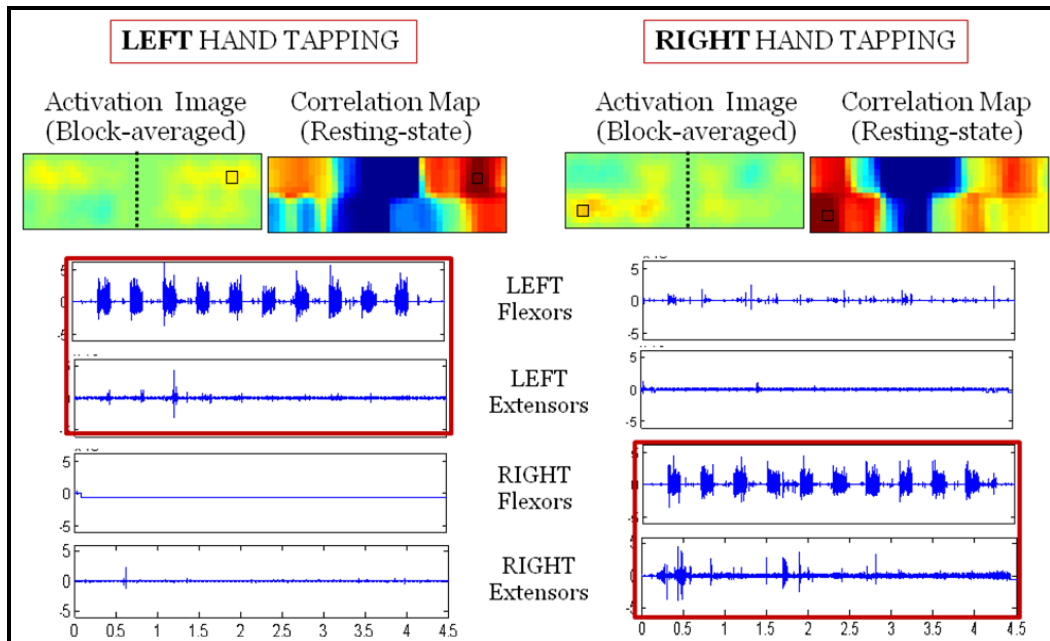
Figure 3.4 Activation images, correlation maps and EMG responses
of left and right hand tapping for CP 2

CP 3-Right paretic (Fig. 3.5): Again the right hand of this subject was paretic due to a deformation in the left motor cortex of the brain. When this subject performed finger tapping with his healthy left hand, a strong bilateral activation was observed. The resting-state correlation map also indicated a high degree of inter-hemispheric connectivity supporting the activations observed. The EMG responses from the left flexors (maroon-bordered) indicated the tapping epochs. Also there was some activity recorded from the non-tapping right hand which might be due to mirror movements. So these movements could have contributed to some extent to the activation seen on the ipsilateral left hemisphere. However, the paretic hand tapping resulted in a contralateral activation (minimally bilateral) of the motor cortex. The functional connectivity maps also prove that there were no neuronal connections between the two hemispheres. The EMG responses of the paretic hand (maroon-bordered) showed the inability

of the subject to perform equally in comparison of the healthy hand. No EMG activity was recorded from the non-tapping hand this time. Thus in spite of the left hemisphere being the damaged hemisphere, it showed contralateral activation similar to a healthy brain.
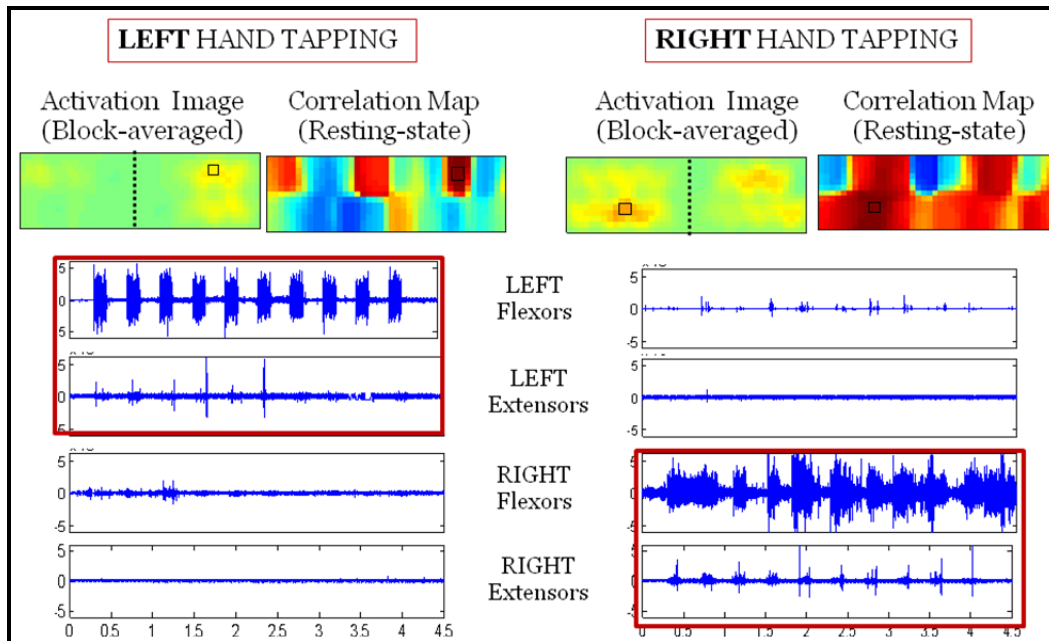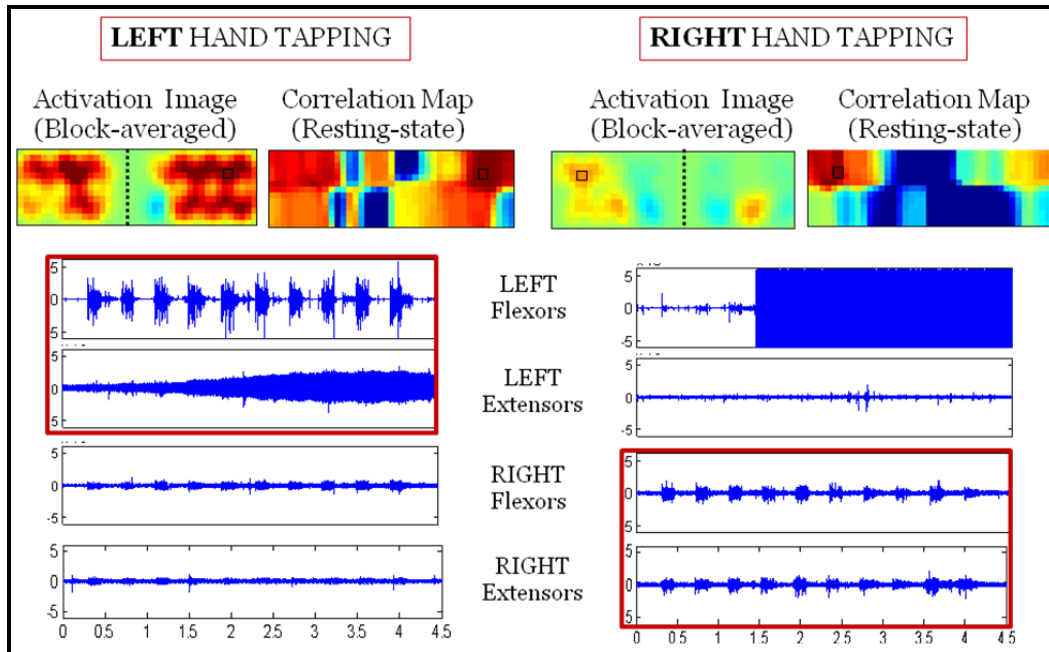

Figure 3.5 Activation images, correlation maps and EMG responses
of left and right hand tapping for CP 3

CP 4-Left paretic (Figure 3.6): The left hand of this subject was paretic due to a deformation in the right motor cortex of the brain. Similar to the subject CP3, this subject demonstrated bilateral activations during the healthy right hand finger-tapping which was confirmed by the correlation maps. Also when this subject performed finger tapping using th paretic left hand, a contralateral activation (minimally bilateral) was observed. The resting-state correlation map also indicated no interhemispheric connections thus supporting the activations observed. The EMG responses were recorded only from the tapping hand during both the protocols.
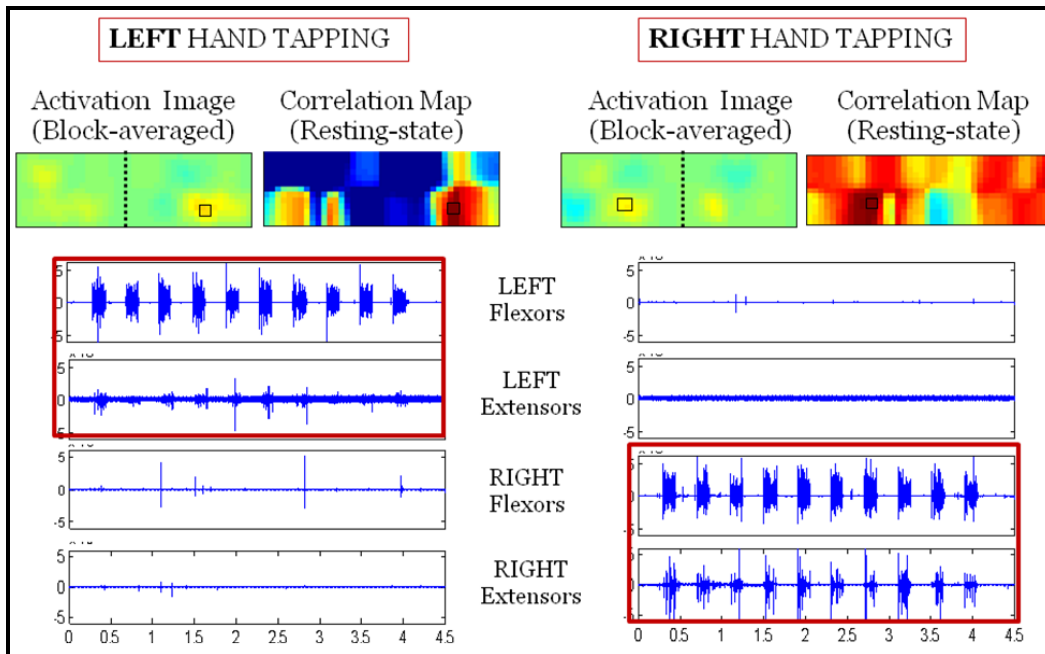
Figure 3.6 Activation images, correlation maps and EMG responses
of left and right hand tapping for CP 4

In conclusion, it can be seen from the functional activation images and the functional connectivity maps that each case of CP has a different pattern of activation and connectivity.

3.3.3 EMG co-validation

In principle, the paretic hand of the CP patients is inefficient in performing daily tasks as compared to the healthy hand. The efficiency with which they performed tasks using the paretic hand was evaluated using the MACS and SHUEE scoring systems [42]-[44]. Using MACS they were classified on a scale of 1-3 (1 being the best) and a percent scale was employed for SHUEE scoring. EMG electrodes in our study recorded the muscle activity of the hand muscles while performing the task. It is however important to validate the EMG responses of the CP subjects with the MACS and SHUEE evaluations to assess the degree of CP affliction.

59

The EMG response of paretic hand was compared with that of the healthy hand to examine the difference in tapping ability of the paretic hand. A factor 'L' was defined as a parameter to compare between the two hands as follows:

$$L = [rms\ (NP) - rms\ (P)] / [rms\ (NP) + rms\ (P)]$$

where, NP = EMG response of non-paretic (healthy) hand during tapping

P = EMG response of paretic hand during tapping
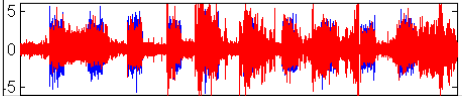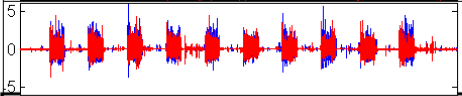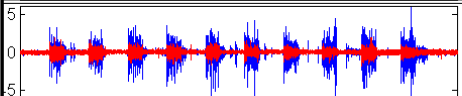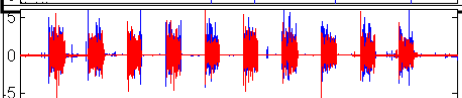
rms = Root Mean Square of the real-time EMG signal

Hence the following possibilities would exist depending on the rms values of EMG signals:

a) L = 0 implies P = NP. The paretic hand's ability is comparable to that of the non-paretic's.

b) L > 0 implies P < NP. The paretic hand's weaker as compared to the non-paretic.

c) L < 0 implies P > NP. The paretic hand's better than the non-paretic.

The following table lists the hemiparesis, MACS and SHUEE scores of each CP subject. Also the EMG response of paretic hand (red) is juxtaposed on that of the non-paretic hand (blue) to visually determine the difference between the two. The L factor has been computed as well.

Table 3.1 EMG response co-validation (using L factor) with MACS
and SHUEE scores for CP

Sub	Hemi paresis	MACS Score	SHUEE Score	Non-Paretic and Paretic hand finger tapping EMG Response	L
1	Right	1	100%		-0.14
2	Right	1	100%		0.06
3	**Right**	**2**	**72%**		**0.28**
4	Left	1	100%		-0.02

60

In case of CP 1, CP 2 and CP 4 who had MACS score of 1 and a perfect SHUEE score, the L were computed to be -0.14, 0.06 and -0.02 respectively indicating that the paretic hand was not very badly affected as compared to the non-paretic. However in case of CP 3 with MACS of 2 and SHUEE of 72%, L was about 0.3 which was greater than 0 indicating that the paretic hand was way worse than the non-paretic hand in performing tasks. Thus using the L factor, the EMG responses were co-validated with the MACS and SHUEE scores to determine the degree of CP severity.

<u>3.4 Illustration of simultaneous DOI / fMRI</u>

3.4.1 Why DOI and fMRI?

Both DOI and functional Magnetic Resonance Imaging (fMRI) are functional imaging modalities that measure cerebral hemodynamics. The Blood Oxygen Level Dependent (BOLD) signal of fMRI is known to be a combination of various vascular parameters, among which Deoxy-Hb is argued to be a major contributor. Hence the fMRI BOLD signal is very comparable with Oxy-Hb and/or Deoxy-Hb of DOI. Also fMRI is indeed the gold standard in functional neuroimaging. Hence by comparing the DOI responses with fMRI, it would cross-validate the findings of DOI. Functional MRI is equipped with a very high spatial resolution but limited by a low temporal resolution. On the other hand, DOI has a very high temporal resolution and a modest temporal resolution. Thus to integrate the best aspects of both the imaging modalities, it is important to study the relationship between the two and then use them simultaneously to get the best results. We ideally plan to use the integrated multimodality approach to study the brain activations and connectivity in CP patients.

3.4.2 MRI data acquisition parameters

A whole- brain high resolution fMRI data was acquired with an echo-planar imaging sequence in the Head First Supine position. The TR used for the study was 2 sec. A field of view (FOV) of 220.000 mm (ap) X 137.600 mm (fh) X 220.000 mm (rl) was chosen. The maximum number of slices/locations was 43 and the maximum number of dynamics was 225 to ensure that the entire brain was covered.

For anatomic reference a T1-weighted whole brain MPRAGE sequence was employed. The TR was set to 8.190 msec. The FOV was set to be 204 mm (ap) X 256(fh) mm X 160 mm (rl). The maximum number of slices/locations was 160.

3.4.3 Experimental setup

The CW-5 imager was placed in the MRI console room. All the sources and detector fibers were wrapped in a sleeve and passed as one long bundle into the scanner room through the wave guide into the MRI Scanner Room (refer fig. 3.7). An Achieva 3.0T (Philips Medical Systems) scanner was used for MRI scanning. The exposed source fibers (without the casing) and the detector fibers (with the casing) are MRI compatible. Then the DOI probe was setup on the subject's head as discussed in section 3.2.2. Vitamin E capsules that acted as MR contrast were attached to the top of each optode for DOI source-detector localization. The subjects were then instructed to watch a visual display mounted on the top of the MR head-coil above the subject's eyes. On the display the instructions to tap or rest were shown. The subject was given headphones to receive instructions from the MR personnel in the console room and a squeeze ball to report any kind of emergency situation.
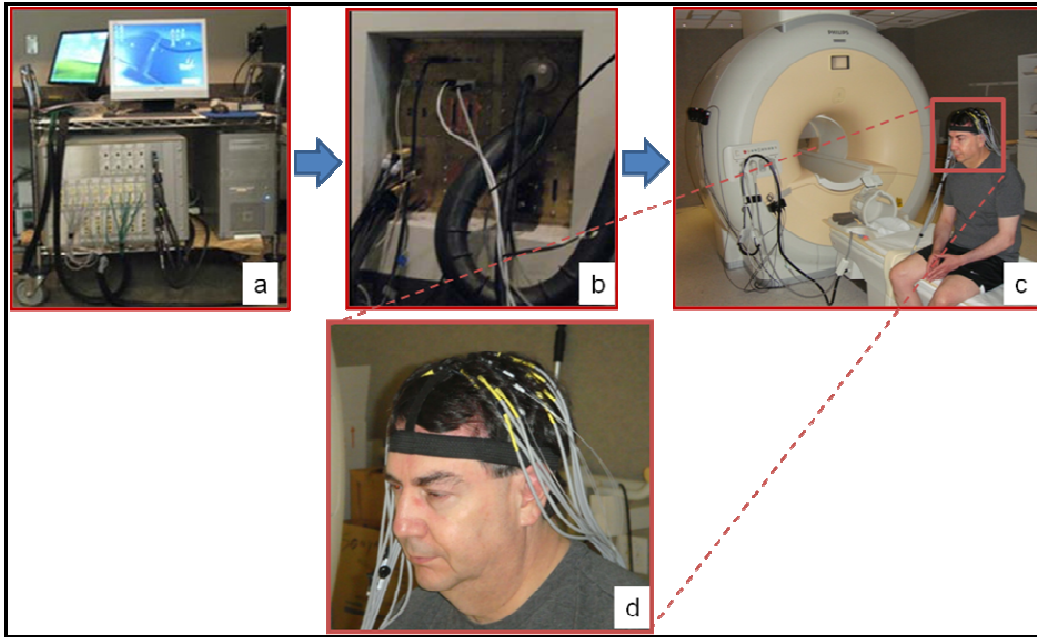
Figure 3.7 Experimental setup for simultaneous DOI/fMRI (a) DOI imager (b) waveguide
(c) MRI scanner with subject (d) subject with DOI probe on head

After shimming of the magnetic coils, an echo planar imaging (EPI) sequence was run
for both of the finger tapping protocols. The protocol described in section 3.2.3 was used for
this multi-modality imaging. Then the T1-weighted MPRAGE image sequence was run for
anatomic reference.

3.4.4 Data processing and analysis using AFNI

All the MRI data was pre-processed using commercially available software -Analysis
of Functional Neuro Images (AFNI). Pre-processing is an important step in functional image
analysis which helps in removing any variability in data that is not due to the experimental task.
There is no standard pipeline for processing fMRI data. The acquired MRI data were pre-
processed in a series of following steps [46]:

63

1. File conversion *(to3d)*: This command is used to create AFNI datasets. The images obtained from the MRI Scanner are in .PAR and .REC format. The to3d command converts the scanner files into .BRIK and .HEAD files that are read and analyzed using AFNI.

2. Mask Generation *(3dAutomask)*: This command masks out the non-brain parts in the image and extracts only the brain regions.

3. Detecting outliers *(3dToutcount)*: This command detects outliers in a sequence of images and checks for image quality. After detecting them, the corresponding points can be censored.

4. Volume registration *(3dvolreg)*: It is essential to ensure that all the acquired data volumes are properly aligned and motion artifacts are corrected for all the possible head motions during the scan time. One of these position-matched functional volumes is chosen as the "base" volume (usually the one closest to the anatomical scan), and all other functional volumes are registered to it. Registration is done at the image level, for example, first image from all the volumes are registered to first image from the base volume.

5. Piecewise linear detrending *(3dTcat)*: The purpose of detrending is to remove any slow drifts in the data, which could be due to physiological or instrument noise.

6. Smoothening *(3dmerge)*: It essentially blurs or smoothes the data by running a low pass filter.

7. Ideal Response *(Waver and 1dplot)*: After the data has been pre-processed, our aim is to localize the area of activation on the 3Dvolumetric data. For our block design, we use linear regression analysis with a single regressor. This is done in multiple steps. Firstly, a regressor that models the hemodynamic response during the task periods is generated. A '.txt' stimulus file that contains a single column of 0's (indicating rest) and 1's (indicating stimulus) is created

that represents tasks and rest respectively. The number of 1's or 0's in the file should be equal to the number of TR's (time of repetition).

The stim file obtained consists of a train of square pulses at the stimulus intervals. But, a typical hemodynamic response has a different behavior as compared to a square pulse. The hemodynamic response function (HRF) is convolved with the stimulus train to obtain a lagged regressor which is a better representation of the hemodynamic response forming the ideal response. The ideal response is generated using the Waver function in AFNI. Waver takes the input stim file, and places a standard hemodynamic response at the beginning of every TR containing a 1. The parameters (delay, rise time etc.) of the HRF that waver uses can be modified using the option – GAM.

8. Regression Analysis *(3dDeconvolve)*: After obraining the ideal response, linear regression analysis is performed for each and every voxel time series in the functional data. The function calculates the deconvolution of a measurement 3d+time dataset with a specified input stimulus time series. Second order polynomial fit was done using the polort 2 option. The number of the input regressors (i.e.1), the file and name of the input regressors are important parameters that are specified using this function. The options –rout and –fout are used to specify what is required in the output dataset. Output image consists of an AFNI 'bucket' type dataset containing the least squares estimates of the linear regression coefficients, f-statistics for significance of the individual input stimuli.

9. Co-registration *(3dAllineate)*: It is used to co-register the anatomical and functional images. This helps in volume-matching of the two scans.

10. Overlay: In order to view activation in specific voxels a set of parameters have to be set in the AFNI window. The Olay and the Thr tab are used to specify the Regression Coefficients and the f-statistics of the regressor respectively. The intensity color bar is set to 2.

The value chosen on the threshold slider is determined empirically. This value is chosen such that activation is obtained only in the region of interest. Once the parameters are set, the activation map is superimposed on the anatomical image to view the exact areas of activation. The underlay image is changed to the anatomical image using the switch underlay command. The overlay image is set to the functional image using the Switch Overlay command. The Overlay image can be viewed by checking the See Overlay Tab. The overlay step is done for both the protocols; using the respective functional image as the overlay image with the anatomical image as the underlay image.

3.4.5 Results

3.4.5.1 Spatial correlation

In DOI, the channel that showed spatial pattern of motor activation was identified. The ROI in DOI images was observed around optode X7 (i.e. X7→O14, and X7→O15) during left hand finger tapping. In figure 3.8 (a) to (c) display the DOI images of Oxy-Hb, Deoxy-Hb and Total-Hb concentrations, respectively and (d) to (f) show the fMRI images in axial, sagittal and coronal views, respectively. Both DOI and fMRI showed distinct activation around optode X7. The location of the vitamin E capsules in each of the views of the fMRI data helps us identify the optical probe location in the MRI Scans. A couple of source detector positions have been marked on the fMRI data. Hence, there is exists a fairly good spatial correlation between the two modalities.
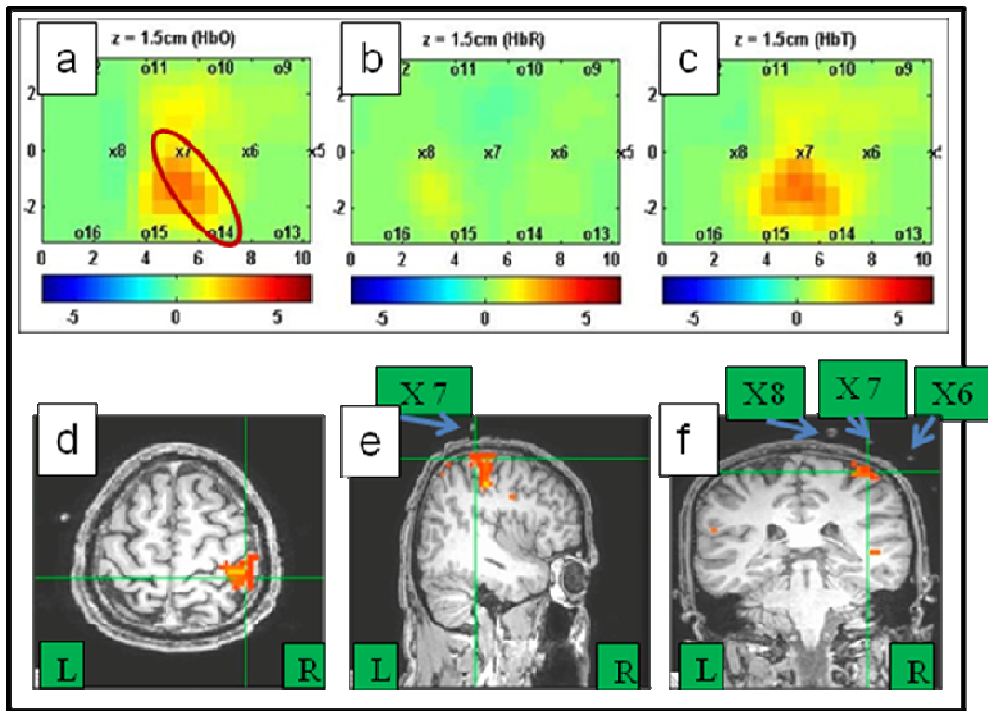
Figure 3.8 Left hand tapping. Spatial activation in DOI: (a) Oxy-Hb (b) Deoxy-Hb
(c) Total-Hb; and fMRI: (d) axial view (e) sagittal view (f) coronal view

During the right hand tapping, the ROI in DOI images was observed around optode X3 (i.e. X3→O2, and X7→O6). Similarly, figure 3.9 (a) to (c) display the DOI images of Oxy-Hb, Deoxy-Hb and Total-Hb concentrations, respectively and (d) to (f) show the fMRI images in axial, sagittal and coronal views, respectively. Both DOI and fMRI showed distinct activation around optode X3. Hence, there is exists a fairly good spatial correlation between the two modalities.
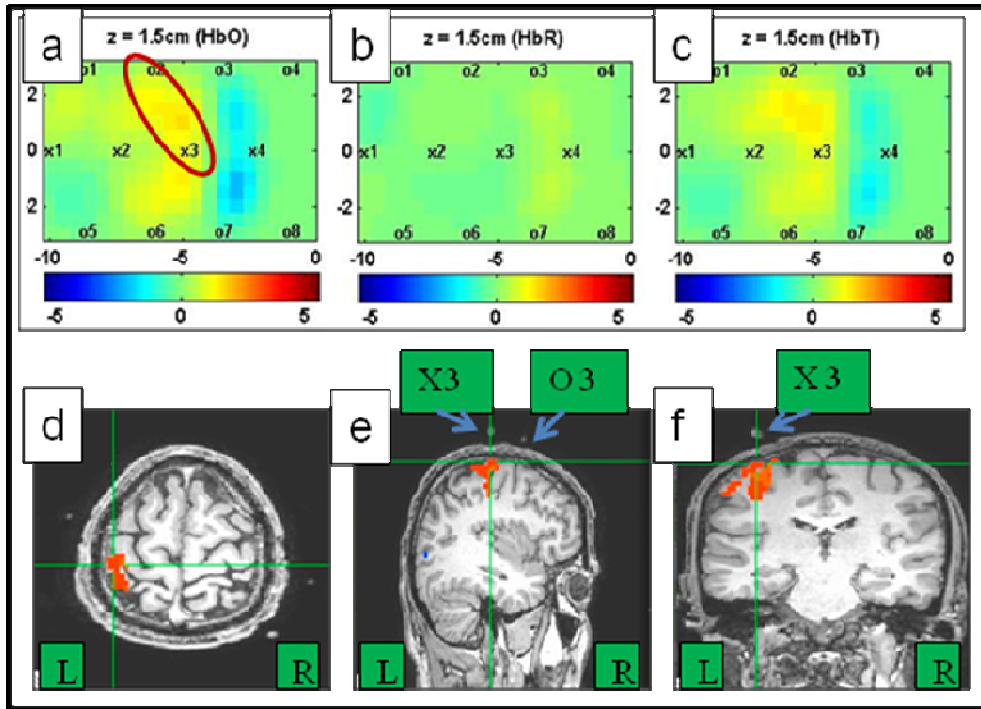
Figure 3.9 Right hand tapping. Spatial activation in DOI: (a) Oxy-Hb (b) Deoxy-Hb
(c) Total-Hb; and fMRI: (d) axial view (e) sagittal view (f) coronal view

3.4.5.2 Temporal correlation

Figure 3.10 below shows the temporal pattern of motor activation from subject #1 during left- and right-hand finger tapping (15-sec tapping plus 25-sec relaxation). For DOI data, four channels around optode X7, i.e. X7→O10, X7→O11, X7→O14, and X7→O15 were plotted consistent with the spatial activation images. The four curves showing initial increases correspond to changes in Oxy-Hb concentration, and the four curves showing initial decreases result from changes in Deoxy-Hb concentrations during (a) left-hand tapping and (c) right-hand tapping. The change in BOLD signal obtained after ROI averaging is plotted in (b) for left-hand tapping and (d) for right-hand tapping. The x axis represents the duration of the block of protocol and the y axis the change in concentration (Molar) for Oxy-Hb, Deoxy-Hb and the change in BOLD signal (a.u) respectively.

68

The time-to-peak or the maximum Oxy-Hb concentrations as well as minimum Deoxy-Hb concentration changes took place at about 10-sec. Also in case of BOLD signal, the time-to-peak was observed at about 10 sec for both the protocols. Overall, the results from both DOI and fMRI are in good agreement.
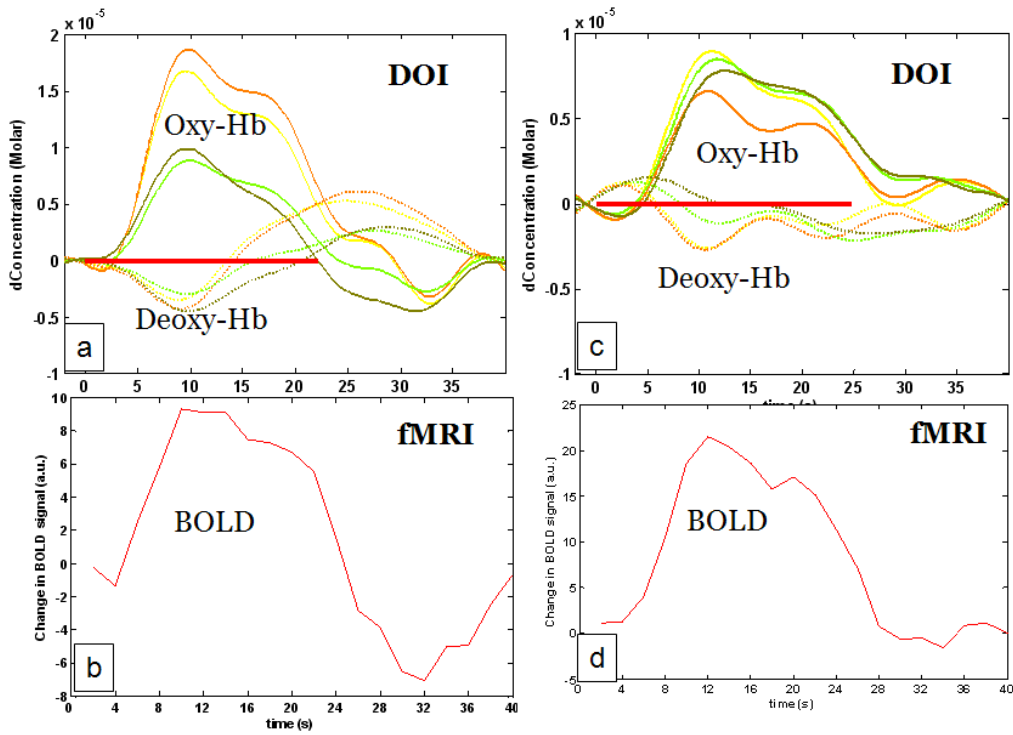
Figure 3.10 Temporal activation during Left hand tapping (a) DOI (b) fMRI;
And during Right hand tapping (c) DOI (d) fMRI

Thus the feasibility of a multimodality imaging using DOI / fMRI was tested positive with the results from both being highly consistent, spatially and temporally, from Subject 1.

CHAPTER 4

DISCUSSION AND CONCLUSIONS

4.1 rTMS / DOI study

TMS induced a bilateral decrease in Oxy-Hb concentrations and generated strong inter-hemispheric effects in motor/prefrontal cortices. Gaining a better understanding of how different treatment parameters using TMS, as a therapeutic tool, interact to produce clinical outcome is critical to optimizing the effectiveness the treatment. Evaluating the reactivity and connectivity of superficial cortical structures with simultaneous rTMS/DOI could inform which treatment parameters are most likely to work. As a potential example, suppose patients with major depressive disorder are found to have a variable degree of prefrontal activation and connectivity with rTMS. This degree of activation and connectivity may predict which parameters are most likely to produce remission of depressive symptoms. The rTMS/DOI could measure that degree of activation and connectivity to help determine which parameters were most likely to relieve the depressive symptoms [90].

4.2 CP-DOI study

Healthy controls showed contralateral motor activation during the finger-tapping task, whereas most of the CP patients showed bilateral activation. With the growing age, the CP patients developed cortical reorganization that caused a difference in the brain excitability and connectivity as compared to controls. In order to improve the child's ability to use his impaired limbs and increase the efficiency of muscle movement by using physical, occupational and

70

constraint-induced therapies or rehabilitative interventions, it is however important to diagnose and prognose the CP patients. By better understanding the changes in the excitation and connectivity in CP using DOI, the effect of these improvement techniques on the brain can be monitored. Multimodality DOI/ fMRI can result in better imaging of the brain hemodynamics with higher spatial and temporal resolution.

4.3 Future work

Functional connectivity analysis should be included in all neuroimaging studies for the basic understanding of brain circuits. rTMS / DOI should be studied in case of depressed patients to evaluate the differences in the cortical excitability and functional connectivity in them as compared to healthy controls. A simultaneous DOI/fMRI multimodality approach should be utilized in cerebral palsy patients to better understand the cortical reorganization and its underlying mechanisms. The present study included the data from only 1 subject. Hence, including a larger subject pool would increase the statistical power of the study for better applications.

APPENDIX A

DOI IMAGER: CW-5 SPECIFICATIONS

CW5 Specifications

Transmitters: Laser Sources

Number of sources...24
Type of source...Laser
Source wavelengths...690 and 830 nm
Optical Output Power per source..................................... 9 mW, 3 mW
Output control Capability modulation.............................On/Off, Square-
wave Connector type..Optical SMA

Receivers: Detectors

Number of receivers... 24
Type of receiver.. Avalanche Photo Diode Photo
sensitivity.. 0.5 A/W @ 800 nm
Gain Range... -12 To +84 dB
Optical bandwidth... 400-1000 nm
Signal bandwidth... 16 kHz
Control capability.. On/Off & programmable Gain
Connector type.. Optical SMA

External Remote Control Details:

Electrical Interface... Serial
Control Language... Proprietary
Data bit rate.. 5 kHz

General Physical Details (approximate as shown in photograph):

Input power...10V AC 60 Hz @ 2.5A
Operating Temperature..0 to 40 C
Storage Temperature...-20 to 60 _C
Humidity... 5 to 95 % noncondensing
Dimensions with...Length 20 inches Enclosure
Width 20 inches
Height 17 inches Rack Mountable 19
"width Weight.. 100lbs in enclosure

APPENDIX B

DOI DATA PROCESSING SOFTWARE: HOMER

HomER (Hemodynamic Evoked Response) is a graphical user interface for visualization and analysis of DOI data. It is a data analysis program initiated by the Photon Migration Imaging lab at the Massachusetts General Hospital (MGH) that allows for basic signal processing, linear modeling and image reconstruction DOI data of brain function. HomER can be divided in to 4 sub sections: Section-1: Signal Processing, Section-2: Response Processing, Section-3: Image Reconstruction, Section-4: Region of Interest Analysis.

1: Signal processing

This section of HomER plots the raw data and probe geometry. It contains tools for filtering time-courses with band-pass filters and principal component analysis. PCA helps in removal of systemic fluctuation and artifact.

2: Response Processing

This section of HomER is dedicated for analyzing functional hemodynamic responses. It supports block-designed and event-related paradigms. The hemodynamic response curves are displayed as per the selected optode location, which helps in localization of activity. Responses can be analyzed for entire protocol in real-time or can be averaged over multiple epochs.

3: Image Reconstruction

This section provides with various options for basic image reconstruction including backprojection and other regularized inversion techniques. It is capable of reconstructing both optical density and hemoglobin concentration images. The response time for reconstruction can be varied with the help of Slide bar, allowing better control over image reconstruction. The

imaging parameter control menu provides the options for varying the absorption and scattering coefficients, the voxel sizes and reconstruction depths.

4: Region of Interest Analysis

In this section one can perform Region-of-Interest (ROI) analysis. ROI averages can be calculated for individual subjects or group of subjects and across multiple sessions. ROIs can be defined by source-detector channel or within the reconstructed image. It calculates the Hemodynamic Response Function (HRF) for the selected region. Comparison between response functions of various subjects can also be done in this section.

REFERENCES

[1] Huppert TJ, Hoge RD, et al. (2006): Quantitative spatial comparison of diffuse optical imaging with blood oxygen level-dependent and arterial spin labeling-based functional magnetic resonance imaging. Journal of Biomedical Optics 11(6), 064018.

[2] Gibson AP, Hebden JC and Arridge SR (2005): Recent advances in diffuse optical imaging." Phys. Med. Biol. 50, R1–R43.

[3] Anas N.: NIRS-Defining its Role in Pediatric Emergency Care.

[4] http://www.scholarpedia.org/article/Near_infrared_imaging

[5] Boas D, Dale A, and Franceschini MA (2004): Diffuse optical imaging of brain activation: approaches to optimizing image sensitivity, resolution, and accuracy," Neuroimage, vol. 23, pp. S275-S288.

[6] Cope M and Delpy DT (1988): System for long-term measurement of cerebral blood flow and tissue oxygenation on newborn infants by infra-red transillumination. Med. Biol. Eng. Comput., vol. 26, pp. 289-294.

[7] Ziemann U, Paulus W, Nitsche MA, et al. (2008): Consensus-Motor cortex plasticity protocols. Brain Stimulation 1(3):164-182.

[8] Thickbroom GW (2007): Transcranial magnetic stimulation and synaptic plasticity-experimental framework and human models. Exp Brain Res 180(4):583-593.

[9] Kozel FA, Tian F, Dhamne S, et al (2009): Using simultaneous repetitive Transcranial Magnetic Stimulation/functional Near Infrared Spectroscopy (rTMS/fNIRS) to measure brain activation and connectivity. Neuroimage 47:1177-1184.

[10] http://www.neuronetics.com

[11] Pridmore S: Download of Psychiatry, Chapter 29. Last modified: November, 2007

[12] http://www.magstim.com

[13] Newport R. Techniques in cognitive neuroscience: TMS.

[14] Siebner HR, Bergmann TO, et al (2009): Consensus paper- Combining transcranial stimulation with neuroimaging. Brain Stimulation 2, 58–80.

[15] George MS, Bohning DE (2002): Measuring brain connectivity with functional imaging and transcranial magnetic stimulation. In: Neuropsychopharmacology, Fifth Generation in Progress.

[16] Girouard H and Iadecola C (2006): Neurovascular coupling in the normal brain in hypertension, stroke, and Alzheimer disease. J. Appl. Physiol., vol. 100, pp. 328-335.

[17] Filosa J and Blanco V (2007): Neurovascular coupling in the mammalian brain," Exp. Physiol., vol. 92.4, pp. 641-646.

[18] Paemeleire K (2002): The cellular basis of neurovascular metabolic coupling," Acta neurol. Belg., vol. 102, pp. 153-157.

[19] First M, Spitzer R, Williams J, Gibbon M (1995): Structured clinical interview for DSM-IV (SCID). Washington, D.C.: American Psychiatric Press.

[20] Keel JC, Smith MJ, Wassermann EM (2001): A safety screening questionnaire for transcranial magnetic stimulation. Clin Neurophysiol 112:720.

[21] CW5 user manual.

[22] Personal communication with Mark Riehl 09/2009.

[23] Borckardt JJ, Nahas Z, et al. (2006): Estimating resting motor thresholds in transcranial magnetic stimulation research and practice: a computer simulation evaluation of best methods. J. ECT. 22, 169–175.

[24] http://www.nmr.mgh.harvard.edu/PMI

[25] Friston KJ (1993): Functional and effective connectivity in neuroimaging: a synthesis. Human Brain Mapping 2:56-78.

[26] Reiss PT (2008): Inferring Group Differences in Brain Connectivity from Functional Magnetic Resonance Images. IMS New Researchers Conference; Boulder, Colorado

[27] Paus T, Jech R, Thompson CJ, et al (1997): Transcranial magnetic stimulation during positron emission tomography: A new method for studying connectivity of the human cerebral cortex. J of Neuroscience 17(9):3178-3184.

[28] Rogers BP, Morgan VL, Newton AT and Gore JC (2007): Assessing Functional Connectivity in the Human Brain by FMRI. Magn Reson Imaging 25(10):1347–1357.

[29] Li K, Guo L, Nie J, Li G, Liu T (2009): Review of methods for functional brain connectivity detection using fMRI. Computerized Medical Imaging and Graphics 33: 131–139.

[30] Cao J, Worsley KJ (1999): The geometry of correlation fields, with an application to functional connectivity of the brain. Ann Appl Probab 9:1021–57.

[31] White BR, Snyder AZ, Cohen AL, et al (2009): Resting-state functional connectivity in the human brain revealed with diffuse optical tomography. NeuroImage.

[32] Cordes D, Haughton VM, et al. (2001): Frequencies contributing to functional connectivity in the cerebral cortex in resting-state data. Am J Neuroradio 22: 1326-1333.

[33] Soot A, Tomberg T, Kool P, et al. (2008): Magnetic resonance imaging in children with bilateral spastic forms of cerebral palsy. Pediatr Neurol, vol. 38(5), 321-328.

[34] Romantseva L (2004): Neuroimaging in Cerebral Palsy. J Pediatr, 145:S19-S27.

[35] Kra¨geloh-Mann I, Cans C (2009): Cerebral palsy update, Brain Dev. in press.

[36] Shapiro BK (2004). Cerebral palsy: A reconceptualization of the spectrum. J Pediatr; 145 (Suppl.):S3-7.

[37] Johnston MV and Hoon AH, Jr. (2006): Cerebral palsy. Neuromolecular Med, vol. 8(4): 435-450.

[38] Back SA (2006): Perinatal white matter injury: the changing spectrum of pathology and emerging insights into pathogenetic mechanisms. Ment Retard Dev Disabil Res Rev, vol. 12(2): 129-140.

[39] Accardo J, Kammann H, Hoon HA (2004): Neuroimaging in cerebral palsy. J Pediatr; 145 (Suppl.):S19-27.

[40] Trivedi R, Gupta RK, Shah V, Tripathi M, et al. (2008): Treatment-Induced Plasticity in Cerebral Palsy: A Diffusion Tensor Imaging Study. j.pediatrneurol :0887-8994.

[41] Kulak W, Sobaniec W (2004): Comparisons of right and left hemiparetic cerebral palsy. J pediatrneurol. 31: 101-108.

[42] Eliasson AC, Krumlinde-Sundholm L, et al. (2006): The Manual Ability Classification System (MACS) for children with cerebral palsy: scale development and evidence of validity and reliability. Developmental Medicine and Child Neurology, vol. 48(7): 549-554.

[43] Morris C, Kurinczuk JJ, et al. (2006): Reliability of the manual ability classification system for children with cerebral palsy. Developmental Medicine and Child Neurology. vol. 48(12): 950-953.

[44] Gromley ME, Gaebler-Spira, and Delgado MR (2001): Validation of the Shriners Hospital for Children Upper Extremity Evaluation (SHUEE) for children with hemiplegic cerebral palsy. The Journal of Bone and Joint Surgery 58: 326-333.

[45] Huppert TJ, Franceschini MA and Boas DA (2006): HomER- A graphical interface for functional NIRS analysis.

[46] http://afni.nimh.nih.gov/afni

BIOGRAPHICAL INFORMATION

Sameer C. Dhamne was born on April 3, 1986 in Mumbai, India. He earned his Bachelor of Engineering degree in May 2007 from the University of Mumbai, India. Right after his bachelor's he took up graduate studies from the joint program in Biomedical Engineering at the University of Texas at Arlington and University of Texas Southwestern Medical Center at Dallas commencing in fall 2007. By working on multiple projects during his thesis, he has gained immense technical and clinical research experience in the areas of neuroimaging, signal and image processing. He plans to join a medical device industry with aims to extending his curriculum and research expertise to real-world clinical applications.